DOCTORAL DISSERTATION PREPARED IN THE INSTITUTE OF PHYSICS OF THE JAGIELLONIAN UNIVERSITY SUBMITTED TO THE FACULTY OF PHYSICS, ASTRONOMY AND APPLIED COMPUTER SCIENCE OF THE JAGIELLONIAN UNIVERSITY

Test of T, P and CP Symmetry in the decay of ortho-Positronium using the J-PET detector

Juhi Raj

Supervised by:
Prof. dr. hab. Paweł Moskal

Auxiliary Supervisor: dr. Eryk Czerwiński

Kraków, Poland
2022

DECLARATION

Wydział Fizyki, Astronomii i Informatyki Stosowanej,
Uniwersytet Jagielloński

Oświadczenie

Ja niżej podpisana Juhi Raj doktoranta (nr indeksu:1142019) doktorantka Wydziału Fizyki, Astronomii i Informatyki Stosowanej Uniwersytetu Jagiellońskiego oświadczam, że przedłożona przeze mnie rozprawa doktorska pt.„Test of T, P and CP Symmetry in the decay of ortho-Positronium using the J-PET detector", jest oryginalna i przedstawia wyniki badań wykonanych przeze mnie osobiście, pod kierunkiem prof. dr. hab. Pawła Moskala oraz dr. Eryka Czerwińskiego. Pracę napisałem samodzielnie.

Oświadczam, że moja rozprawa doktorska została opracowana zgodnie z Ustawą o prawie autorskim i prawach pokrewnych z dnia 4 lutego 1994 r. (Dziennik Ustaw 1994 nr 24 poz. 83 wraz z późniejszymi zmianami).

Jestem świadoma, że niezgodność niniejszego oświadczenia z prawdą ujawniona w dowolnym czasie, niezależnie od skutków prawnych wynikających z ww. ustawy, może spowodować unieważnienie stopnia nabytego na podstawie tej rozprawy.

Podpis:

. . . . . .

Kraków, dnia

. . . . . .

"The study of physics is also an adventure. You will find it challenging, sometimes frustrating, occasionally painful, and often richly rewarding".

- Hugh D. Young.

This thesis is dedicated to my ever-loving **Mother**.

Abstract

Conservation of discrete symmetries plays a fundamental role in the exploration of physics laws in the area of elementary particle physics. CP symmetry violation in the weak interaction was one of the first intriguing discoveries to the particle physics community in this domain. So far, there has not been any experimental evidence of violating discrete symmetries in the charged leptonic sector. This Ph.D. thesis reports the explored sensitivity of testing the T, P and CP symmetries in the charged leptonic sector using the versatile and novel detector, Jagiellonian-Positron Emission Tomograph (J-PET), in the decay of ortho-Positronium. A distinctive research methodology to test T, P and CP discrete symmetries in the decay of ortho-Positronium was formulated from four experiments conducted through 2017-2020 for 122 days. The achieved result showed no asymmetry within the achieved sensitivity of 7×10^{-4}.

Contents

CHAPTER1

INTRODUCTION

This thesis concerns the tests of discrete symmetries using an unique method based on the measurement of the expectation value of a discrete-symmetry odd-operator constructed from the momentum and polarization direction of the annihilation photons from the decay of ortho-Positronium [1]. This measurement was conducted using the first Positron Emission Tomograph (PET) prototype built from plastic scintillators [2–6], capable of multi-photon and positronium [7] imaging [8].

One of the most fundamental concepts in the laws of nature leading to conserving quantities are symmetries [9]. The invariance of a system under a continuous symmetry transformation leads to a conservation law by Noethers' theorem [10]. The discrete symmetries of nature such as charge conjugation (C), parity (P) and time-reversal (T) play an important role in particle physics, especially in calculations of the cross sections and decay rates [11,12]. Composed symmetries, such as CP and CPT, are also considered. It was long thought that CP was an exact symmetry in nature [13]. Since the introduction of the concept of these fundamental discrete symmetries in microscopic systems described by quantum mechanics by E. Wigner in 1931 [14], large efforts have been made to test these symmetries with various systems and interactions. CP-violation was discovered in the neutral kaon system by Christensen, Cronin, Fitch and Turlay, in 1964 [15]. A few years later Kobayashi and Maskawa demonstrated that a third quark generation could accommodate CP violation in the Standard Model by a complex phase in the CKM matrix [16, 17]. Therefore, unexpected violations of symmetries indicate some dynamical mechanism beyond the current understanding of physics.

The CPT theorem reveals the foundation of CPT symmetry conservation requirement, which is equivalent to usage of unitary, local and Lorentz-invariant quantum field theory [18, 19]. CPT contains charge conjugation, and therefore represents a symmetry between matter and antimatter [20]. The amount of CP violation contained in the Standard Model appears to be insufficient for a convincing explanation of the observed prevalence of matter over antimatter in the Universe [21]. For these reasons, discrete symmetry tests remains an interesting experimental research in fundamental physics. As mentioned before, there has been no experimental evidence of violating the discrete symmetries in the charged

leptonic sector [13]. T-symmetry remains to be extremely attractive because one can reverse the direction of the motion in space but one cannot reverse the direction of the elapsing time [22].

In order to study the P, T and CP symmetry violation, the expectation values for the symmetry odd-operators of the non-degenerate stationary states are investigated [23]. Since motion can be reversed, the time-reversal invariance is often referred to as motion reversal symmetry. For such studies, the anti-unitary character of the T-symmetry operator makes the experimental studies of the time reversal invariance more challenging than other symmetries, since it requires abilities of preparing the initial and final states of the process in a fully controlled way [24]. So far, none of the experiments reported limits on the discrete-symmetry violations in the decays of Positronium. The known final state interactions of photons are expected to mimic the symmetry violation at the level of 10^{-9} [25, 26]. All of the previous investigations with Positronium, which tested the discrete symmetries odd operators, were based on the products of photons momenta and Positronium spin vectors [7, 26–28]. The experiment performed as part of this thesis was conducted by taking advantage of properties of the Jagiellonian-Positron Emission Tomograph (J-PET), which enables to determine the momentum direction of the secondary scattered photons [1]. Therefore, using the J-PET detector, P, T and CP symmetry was investigated by searching for the possible non-zero expectation values of one of the operators which is constructed using the momentum directions of the primary and secondary scattered photons originating from the decays of the ortho-Positronium. This thesis reports an improved experimental sensitivity of testing the P, T and CP symmetry in the decay of ortho-Positronium atoms using the J-PET with the discrete symmetry odd-operators [1]. The implemented experimental setup and analysis methods are reviewed in the articles [29–33].

The theoretical principles and experimental searches of discrete symmetries in the Positronium bound system are described in Chapter 2. The details of the extensive experimental measurements conducted with the J-PET detector through 2017-2020 are described in Chapter 3. The signal selection method and the reconstruction of the experimental data are described in Chapter 4. The elaborated systematic error contribution is described in Chapter 5. The result obtained with this experiment is in agreement with the current published result for discrete-symmetry tests in the charged leptonic sector and is thrice more precise [28]. The obtained result shows no discrete symmetry violation visible within the achieved accuracy. Chapter 6 summarises this experiment and describes the future prospects of this experiment with upgraded versions of the J-PET detector.

CHAPTER2

DISCRETE SYMMETRY TRANSFORMATION

2.1 Continuous and Discrete Symmetries

Continuous and discrete symmetry transformations are the two forms of symmetry transformations [10]. Continuous symmetries have parameters that can take any value in a defined range [34]. Discrete symmetries, on the other hand, are identified by a set of discrete values [35]. Bilateral symmetries are discrete symmetry transformations whose two fold operation is the same as no operation [36]. For example, mirror reflection is a bilateral transformation since mirror reflection of a mirror reflection is as good as no reflection as shown in the scheme,

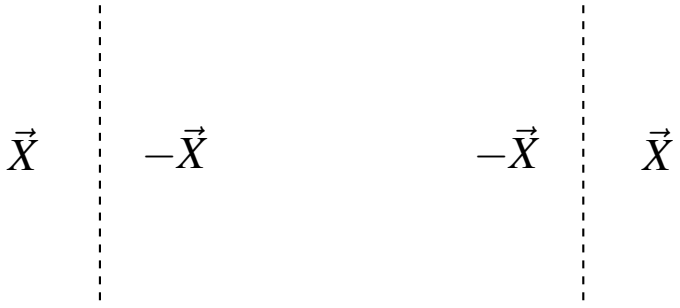

In 3-dimensions, if the mirror is kept parallel to xy-plane, then the reflection will reverse the direction of Z-axis while reflection of this reflected image brings the Z-axis back to its initial configuration. If we denote the bilateral transformation operator which acts on the system S by B then we have,

$$B(BS) = S, \tag{2.1}$$

which means for all bilateral operators, $B^2 = 1$. In the following section we will talk about three kinds of bilateral symmetries namely, parity or spatial inversion (P), charge conjugation (C) and time reversal (T) [37].

2.1.1 Parity - The Left-Right Symmetry, P

Parity transformation refers to the inversion of spatial co-ordinates with respect to the origin, i.e.,

$$\vec{X} \longrightarrow -\vec{X}. \tag{2.2}$$

Hence, parity is a bilateral transformation [38]. Parity is also called left-right symmetry. Under parity operation P, a function $f(\vec{X})$ transforms to $f(-\vec{X})$, and if these two functions are the same up to a sign then the function $f(\vec{X})$ will be said to have definite parity [39].
For example,

$$cos(x) \xrightarrow{P} cos(-x) = cos(x),\ even\ parity, \tag{2.3}$$

$$sin(x) \xrightarrow{P} sin(-x) = -sin(x),\ odd\ parity. \tag{2.4}$$

If $f(-\vec{X})$ and $f(\vec{X})$ are of different forms then the function does not have definite parity. The solutions of parity symmetric physical equations may be of definite parity. In the context of elementary particle physics it becomes necessary to assign such parity quantum numbers to particle states (wave functions) [37]. The parity of the wave function of a single particle state is called its intrinsic parity [40].

The Wu experiment was a particle and nuclear physics experiment carried out by Chien-Shiung Wu, a Chinese American physicist, in partnership with the US National Bureau of Standards' Low Temperature Group in 1956 [38]. The goal of the experiment was to see if conservation of parity (P-conservation), which had previously been proven in electromagnetic and strong interactions, was also true for weak interactions. The weak interaction was found to violate conservation of parity (P-violation) in the experiment. The physics world had not expected this conclusion because parity had previously been thought to be a preserved quantity [41].

2.1.2 Charge Conjugation - C

An operation that changes the sign of the charge is called charge conjugation,

$$C\,|p\rangle = |\bar{p}\rangle\,. \tag{2.5}$$

Symmetry under C implies that interaction of two particles is independent of the sign of their internal quantum numbers and charge [42, 43]. In other words, this symmetry implies interaction of two particles is exactly identical to the interaction of the corresponding antiparticles. Mills and Berko [44] examined C-Symmetry with the annihilation mode ($^1S_0 \rightarrow 3\gamma$) experimentally in 1967. In the situation of three photons emerging symmetrically in the Positronium centre of mass frame (photons emission relative angles equal to 120°, 120°, 120°), the

C-non-conserving ${}^1S_0 \to 3\gamma$ rate must vanish, regardless of the anticipated shape of the C-non-conserving interaction [45]. Mills and Berko looked at the count rate of three photons in three different angle orientations. The branching ratio R of ${}^1S_0 \to 3\gamma$ decays $3\gamma/2\gamma$ was estimated with the best limit so far ($R = 2.6 \times 10^{-6}$ at 68% confidence level [44]).

2.1.3 Time Reversal - T

Reversal in time implies reversing the direction of the time coordinate, i.e.,

$$t \xrightarrow{T} -t. \tag{2.6}$$

Symmetry of a physical system under time reversal simply means that all the processes in the system are reversible [46]. Physical systems involving only strong and electromagnetic interactions are symmetric under all three bilateral transformations listed above. But in nature, other types of interactions, namely, weak and gravitational interactions, exist. Weak interactions are known to violate P as well as T as it will be discussed in the next sections [9, 25, 26].

2.1.4 CPT Theorem

All the known forces or interactions of nature can be traced to four fundamental interactions, namely, gravitational, electromagnetic, strong, and weak. If we take the whole universe as one system, which involves all four kinds of interactions, then surely the system is not symmetric under P, C and T separately because the system violates all three symmetries. Then one may ask, "Is the system symmetric under certain combinations of these transformations?" to which the answer turns out to be "yes". Under the combined operation of all three transformations physical laws remain unchanged. More accurately, invariance under the combined action of C, P and T is a consequence of Lorentz invariance, locality and unitarity of the laws of physics also known as the CPT theorem. Certain consequences of this theorem are:

- the mass of a particle and its anti-particle are exactly the same,
- the total life-time, Δt, of an unstable particle and its anti-particle are exactly the same,
- the magnetic moment is equal and opposite for particle and anti-particle.

For example, masses of electron and positron are exactly same, the life-time of K^+ is same as that of K^-, etc. Till date all the tests for CPT violation have yielded negative results [13].

2.2 Experimental Tests of CP-Symmetry

In the weak interactions, P and C are maximally violated simultaneously, such that the system is symmetric under the combined operation of CP. This is clear from the way fermions transform under P and C operations. In nature only left-handed neutrino ($\nu_{\rm L}$) and right-handed anti-neutrino ($\nu_{\rm R}$) exist, which are CP transforms of each other. Hence, earlier it was thought that though weak interactions violate P and C they still possess CP-symmetry. In 1964, Christenson, Cronin, Fitch and Turlay observed that decay of neutral kaon violating CP -symmetry [47]. Neutral kaons, $\rm K^0$ and $\bar{K}^0$, are produced, for example, in pion-proton collisions via strong interaction,

$$\pi^- p \longrightarrow K^0 \Lambda \tag{2.7}$$

$$\pi^+ p \longrightarrow \bar{K}^0 K^+ p \tag{2.8}$$

and they decay primarily to two-pion and three-pion final states via the weak interaction with two different life-times. Based on the life-times of decays in to these modes, kaons were renamed as K-short ($\tau_{\rm KS} = 0.89 \times 10^{-10}$sec) and K-long ($\tau_{\rm KL} = 5.17 \times 10^{-8}$sec). By conservation of angular momentum and intrinsic parity of pion, it is clear that the two-pion state, $|2\pi\rangle$, has CP = +1 and the three-pion state, $|3\pi\rangle$, has CP = -1. This implies that $|K^0\rangle$ and $|\bar{K}^0\rangle$ are not CP eigenstates, and in fact they transform into each other under CP operation i.e.,

$$|K^0\rangle \xrightarrow{CP} |\bar{K}^0\rangle \tag{2.9}$$

With this property of neutral kaon states the CP eigenstates can be formed as the following linear superpositions,

$$|{K^0}_1\rangle = \frac{1}{\sqrt{2}}(|K^0\rangle + |\bar{K}^0\rangle \qquad CP = +1 \tag{2.10}$$

$$|{K^0}_2\rangle = \frac{1}{\sqrt{2}}(|K^0\rangle - |\bar{K}^0\rangle \qquad CP = -1. \tag{2.11}$$

Earlier ${\rm K^0}_1$ (${\rm K^0}_2$) was identified as $\rm K_S$ ($\rm K_L$), which decays to two (three)-pion or CP-even (odd) state, and CP is conserved. But it was observed that $\rm K_L$ also decays into two-pions, which is CP-even and hence CP is violated. If we take a beam of $\rm K^0$, which is produced by strong interactions, and which can be written as linear superposition of $\rm K_L$ and $\rm K_S$, then the two-pion decay mode of $\rm K_L$ will interfere with that of $\rm K_S$ as a function of time. Further, according to CPT-theorem, CP violation implies T violation, but there is no direct evidence for it in neutral kaon

system. Thus, the source of CP violation is not yet clear and the phenomenon needs better understanding as it may have been responsible for the net baryon number of the present day Universe [9].

2.3 Experimental Tests of Time-Reversal Symmetry

Soon after the discovery of parity violation in experiments following the suggestions of Yang and Lee [48] many physicists considered the possibility of violation of the other discrete symmetries that were discussed earlier. The great Russian physicist L. D. Landau considered the possibility of elementary particles possessing a non-vanishing electric dipole moment (EDM) which would imply the violation of T-reversal invariance [49]. Note however that a complex system like a water molecule does possess an EDM, but this does not come into conflict with T- reversal invariance. There are many atomic systems in which the EDM of elementary particles such as neutrons or electrons can manifest themselves. However, these EDM appear to be very small quantities and there has been no detection of such effects. This implies that experiments must seek higher levels of precision before they can announce a discovery, and it also implies that theoretical scenarios which predict large values of EDM can be constrained or ruled out by the non-observation of EDM. The Standard Model of the electro-weak interaction gives a contribution to the neutron EDM of the order of 10^{-31} to 10^{-33} e cm which, because it is second order in the weak interaction coupling constant, is very small [22]. Rutherford Appleton Laboratories implements a specific technique based on ultra-cold neutrons, where, nuclear reactors serve as copious sources of neutrons which are used for a variety of experiments. Normally these neutrons emerge with a kinetic energy of about 1/40 eV, and are called thermal neutrons. In order to carry out very precise measurements of static and other properties of neutrons, it is necessary to slow them down to very low kinetic energies of the order 10^{-7} eV or even less. Such neutrons are called ultra-cold neutrons and provide an opportunity to carry out highly precise experiments. "The Ramsey resonance technique" can be used to measure with very high precision the precession frequency of ultracold neutrons in a weak magnetic field [50]. The precession frequency will change in the presence of an electric field if the neutron has an EDM. The most recent result give an upper bound of the order of $d_n \leq 10^{-26}$ e cm [51].

2.4 Other Experimental Searches with o-Ps

Interaction between electron-positron pair leads to direct annihilation into photons or creation of a bound state called Positronium [37]. Depending on Positronium's quantum mechanical state, this system decays by the annihilation of e^+ and e^- into photons depending on Positronium's quantum mechanical state $|\Phi_{\mathrm{n,l,m}}(\vec{r})|\mathrm{S},\mathrm{S_z}\rangle$, where the orbital wave function Φ is the hydrogen atom wave function with the electron mass replaced by the reduced mass of the electron-positron pair and where n, l, and m are the usual principle, orbital and magnetic quantum numbers, respectively [52]. The spin is a linear combination of electron and positron spins, of which there are four possibilities:

$$\begin{aligned} &|S=1,S_z=1\rangle = |\uparrow\rangle\,|\uparrow\rangle\,, \\ &|S=1,S_z=0\rangle = \tfrac{1}{\sqrt{2}}(|\uparrow\rangle\,|\downarrow\rangle + |\downarrow\rangle\,|\uparrow\rangle), \\ &|S=1,S_z=-1\rangle = |\downarrow\rangle\,|\downarrow\rangle\,, \\ &|S=0,S_z=0\rangle = \tfrac{1}{\sqrt{2}}(|\uparrow\rangle\,|\downarrow\rangle - |\downarrow\rangle\,|\uparrow\rangle), \end{aligned} \tag{2.12}$$

where $|\uparrow\rangle$ and $|\downarrow\rangle$ denote $\mathrm{S_z} = +\frac{1}{2}$ and $\mathrm{S_z} = -\frac{1}{2}$ for a single electron (positron) [37, 53]. The triplet state is called ortho-Positronium, while anti-aligned singlet state is called para-Positronium [54]. Constrained by conservation laws, the ortho-Positronium state can annihilate only to an odd number of photons, while the para-Positronium state can decay only to an even number of photons [52]. In practice, final states with larger photon numbers are suppressed by few orders of magnitude and the Positronium annihilations are dominated by $p-Ps \to 2\gamma$ and $o-Ps \to 3\gamma$ [55]. The inverse of the decay rates give the mean lifetimes of the states in vacuum:

$$\begin{aligned} \tau_{o-Ps} &= 142\ ns, \\ \tau_{p-Ps} &= 0.125\ ns. \end{aligned} \tag{2.13}$$

Positronium is a purely leptonic state which allows to determine its properties using quantum electrodynamics alone [9, 37, 52]. Thus, Positronium annihilation into photons can be used for tests of discrete symmetries tests involving correlations of photons momenta originating form o-Ps annihilation. [1, 26].

2.4.1 CP searches with o-Ps

In 1973, Kobayashi and Maskawa [17] addressed CP violation in quark systems by pointing to the presence of the complex phase in the quark transition matrix, expanding on Cabibbo's [56] model and implying the existence of three quark generations (at those days only up, down and strange quarks were known but indeed charm, bottom, and top quarks were discovered later). In 2008, Kobayashi and Maskawa were awarded the Nobel Prize for this prediction. Sakharov [43]

has argued that the violations of C and CP symmetries are necessary requirements for the explanation of the observed excess of matter over anti-matter. However, the presently known sources of the CP symmetry violations are still by far too small and can account for only about 10^{-9} fraction of the observed excess of matter over anti-matter [57]. Therefore, many particle physics experiments search for CP symmetry violation effects in hadrons [58, 59]. Other experiments are testing the CP-symmetry violation in processes using purely leptonic systems at the same time [60, 61]. The most recent experiment testing the CP-symmetry in the charged leptonic sector was conducted in the University of Tokyo and reports the present best upper limit on the CP violation in the decays of ortho-Positronium (triplet state of the Positronium) atoms [28]. If CP is violated in the lepton sector, such neutral systems (e.g. Ps, muonium) are good test candidates since the admixture of opposite CP eigenstates will occur. The experimental setup used a 1 MBq ^{22}Na positron source sandwiched between two sheets of thin plastic scintillator. The gamma-rays emitted from ortho-Positronium decay were observed in four LYSO ($Lu_{1.8}Y_{0.2}SiO_5$) crystal scintillators of 30 mm diameter and 30 mm length. The experiment included five runs with different alignments of the LYSO detectors to check systematic effects dependent on the position of the LYSO detectors. The total data acquisition period was about six months. The trigger rates were about 1.3 kHz. During the data acquisition, the turntable was rotated around 30° every hour. Such experiments are based on the separation of the two Positronium states by their very different lifetimes: $\tau(^1S_0) \cong 125$ ps versus $\tau(^3S_1) \cong 142$ ns. The experiment measured the discrete-symmetry odd operator with angular correlation,

$$(\vec{S} \cdot \vec{k_1}) \cdot (\vec{S} \cdot (\vec{k_1} \times \vec{k_2})) \tag{2.14}$$

where, $\vec{S}$ is the spin direction of the ortho-Positronium and $|\vec{k_1}|$ and $|\vec{k_2}|$ are the momenta of the two most energetic annihilation photons. The expectation value (C_{CP}) was determined to be $0.0023 < C_{CP} < 0.0049$ with statistical sensitivity of 2.2×10^{-3}, observing no CP violation, which is at the level of the CP violation amplitude in the K meson. This leaves 6 orders of more statistical sensitivity to be explored in this aspect.

2.4.2 CPT searches with o-Ps

Studies on CPT odd triple correlations,

$$\vec{S} \cdot (\vec{k_1} \times \vec{k_2}) \tag{2.15}$$

where $\vec{S}$ is the spin of the ortho-Positronium, and $|\vec{k_1}|$ and $|\vec{k_2}|$ are the momenta of the two most energetic annihilation photons, were suggested in 1988 by W. Bernreuther, U. Löw, J. P. Ma, and O. Nachtmann [62]. The first measurement of this angular correlation was performed at Ann Arbor [26]. The relation of the

measured asymmetry to the coefficient of the angular correlation was determined by several factors including: the detector acceptance and geometry, the Ps polarization, the 8% background due to badly measured two-photon annihilation events. From a total of 3.5×10^5 events the null result,

$$O_{\mathrm{CPT}} = 0.020 \pm 0.023, \tag{2.16}$$

was obtained for the coefficient of the angular correlation $\mathrm{O_{CPT}}$. In 2003 by P. A. Vetter and S. J. Freedman the sensitivity of this test was improved using the Gammasphere detector [27]. Gammasphere is an array consisting of 110 high purity germanium (HPGe) detectors. Each Ge detector assembly consists of a 7 cm diameter and 8 cm long cylindrical HPGe detector surrounded by six bismuth germanate (BGO) scintillators on the sides and one BGO scintillator at the back [63]. The probability that a detected 511 keV photon deposits its full energy is roughly 15%. In the experiment with Gammasphere, the 0.37 MBq source of ^{68}Ge or ^{22}Na was placed underneath a thin (0.2 mm) plastic scintillator and a hemisphere of silicon dioxide aerogel. Positrons from β decay were identified by around 70 keV energy deposition in the scintillator. The average ortho-Positronium polarization was 21.5% for ^{22}Na and 30.5% for ^{68}Ge. The magnitude of the source polarization is reduced by accepting positrons in a solid angle of 2π. During the 36 day experimental run, the Gammasphere reconstructed around 2.7×10^7 o-Ps$\rightarrow 3\gamma$ annihilation events [27]. The observable measured by the Gammasphere was the asymmetry:

$$A = \frac{N_+ - N_-}{N_+ + N_-} \tag{2.17}$$

where $\mathrm{N_+}$ and $\mathrm{N_-}$ denote number of decays with the normal to the decay plane parallel (+) and antiparallel (-) to the o-Ps spin direction, respectively. The measured asymmetries for each orientation of the decay plane were compared to the Monte Carlo simulation containing a CPT-odd asymmetry and then averaged; with 2.7×10^7 [27] events the measured coefficient was,

$$O_{\mathrm{CPT}} = 0.0071 \pm 0.0062.$$

In the year 2021, the limitations of the previous experiments were overcome by the J-PET detector due to its much higher granularity [7]. During past experiments, the ortho-Positronium decay point was assumed to lie within the aerogel targets, e.g. hemisphere in Gammasphere, and its exact time and spatial coordinates were not reconstructed. In J-PET, however, due to its relatively high angular acceptance [5] and timing resolution [64], a reconstruction of the $o-Ps \rightarrow 3\gamma$ process is possible by means of a new trilateration-based reconstruction method [65]. This method allows for a simultaneous reconstruction of both location and time of the annihilation based on time and interaction position of

gamma quanta in the J-PET detector. Gamma quanta from the $o - Ps \rightarrow 3\gamma$ annihilation travel on a distance between the annihilation point (which needs to be localized) and the detector where the places and times of their interaction are recorded and serve as reference points. An additional constraint is given by the fact that all three photons are produced in a three-body decay and thus their momenta as well as the o-Ps decay point are contained within a single plane in the frame of reference of the decaying Positronium atom. For the experimental realization of triple correlation measurements of the CPT odd-operator as shown in Equation 2.14, a vacuum chamber with walls coated on the inner side with a porous medium for o-Ps production was used. The experiment collected a total of 7.3×10^6 signal event candidates in a continuous 26-day measurement using the described setup with a 10 MBq ^{22}Na positron source. The measure of the observed symmetry is

$$< O_{\mathrm{CPT}} > 0.00025 \pm 0.00036 \tag{2.18}$$

implying no significant asymmetry [7]. The error was dominated by the statistical uncertainty of ± 0.00033. For comparison with the measurements conducted to date [27], a parameter quantifying the level of observed CPT violation $C_{\mathrm{CPT}} \in [0,1]$ can be used, as in the gammasphere experiment discussed above, for which $C_{\mathrm{CPT}} = 1$, corresponds to a maximal asymmetry violating CPT. Correcting the above result for the analysing power <*P*>, the experiment obtained,

$$C_{\mathrm{CPT}} =< O_{\mathrm{CPT}} > /P = 0.00067 \pm 0.00095. \tag{2.19}$$

The reported result is the present best upper limit on the CPT violation in the decay of ortho-Positronium, leaving us 5 orders of more statistical sensitivity to be explored in this aspect.

2.5 P, T and CP symmetry measurement with J-PET

So far, none of the experiments reported simultaneously the T, P and CP symmetry violations in the decays of ortho-Positronium. As discussed earlier, it is the simplest atomic system with charge conjugation eigenstates. This makes it ideal for studies of the discrete symmetries [66]. All of the previous investigations with Positronium, which tested the discrete symmetries, were based on symmetry odd-operators constructed as the products of photons momenta ($\vec{k}_i$) and Positronium spin ($\vec{S}$) vectors as shown in the Table 2.1 [1, 7, 27, 28],

This thesis describes an extended study using another proposed operator [1], taking advantages of properties of the J-PET scanner, which enables to determine

Table 2.1: Discrete symmetry odd-operators using spin orientation of the o-Ps and momentum directions of the annihilation photons

Operator	**C**	**P**	**T**	**CP**	**CPT**
$\vec{S}\cdot\vec{k_1}$	+	−	+	−	−
$\vec{S}\cdot(\vec{k_1}\times\vec{k_2})$	+	+	−	+	−
$(\vec{S}\cdot\vec{k_1})\cdot(\vec{S}\cdot(\vec{k_1}\times\vec{k_2}))$	+	−	−	−	+

the linear polarization direction of photons as shown in Table 2.2.

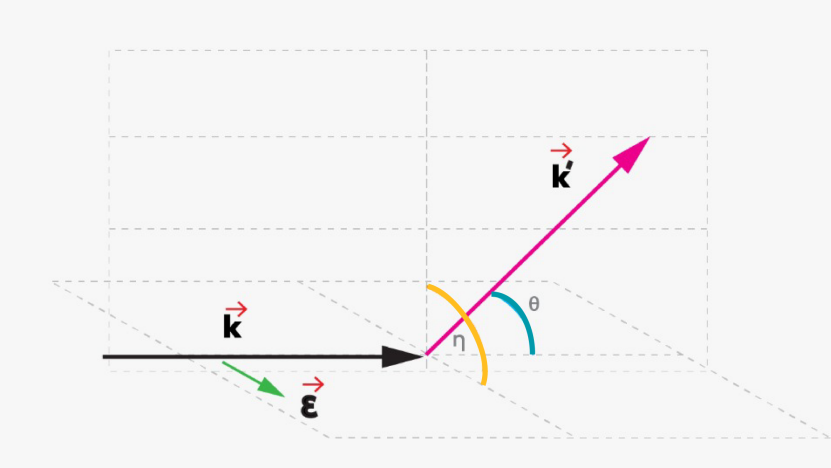

Figure 2.1: The figure describes the interaction of a photon via Compton scattering. The vector $\vec{k}$ denotes incident primary annihilation photon momentum direction and the scattered photon momentum direction is denoted as $\vec{k'}$. The Compton scattering angle is shown as θ. Primary annihilation momenta and scattered momenta form a plane, referred to as the scattering plane. The linear polarization direction of the primary annihilation photon is given as $\vec{\varepsilon} = \vec{k}\times\vec{k'}$. The incident photon momentum ($\vec{k}$) and its linear polarization vector ($\vec{\varepsilon}$) form a second plane, referred to as the polarization plane. The angle between the two planes is denoted by η.

The J-PET scanner being made up of plastic scintillator strips [5, 67], photons from Positronium decay, primarily interact via the Compton effect [6], and thereafter the scatter may interact in various scintillator strips [68]. Since gamma quantum is a transverse electromagnetic wave, Compton scattering is at most likely in the plane perpendicular to the electric vector of the photon [69, 70], and we can determine the direction of its linear polarization ($\vec{\varepsilon}$) of the primary

annihilation photon by constructing [1],

$$\vec{\varepsilon} = \vec{k} \times \vec{k'} \tag{2.20}$$

The vectors $\vec{k}$ and $\vec{k'}$ denote momentum vectors of the gamma quantum before and after the Compton scattering, respectively, as indicated in Figure 2.1. The ortho-Positronium decay plane and the scattering plane for one of the photons are shown schematically in the Figure 2.1. The scatter angle, θ, is between the directions of propagation of the primary annihilation photon $\vec{k}$ and the secondary scattered photon $\vec{k'}$. In order to construct the discrete symmetry odd-operator as discussed in Table 2.2, we measure another angle, α in an ortho-Positronium decay, which denotes the angle between the linear polarization direction of a primary annihilation photon and the momentum direction of another annihilation photon from the same decay event ie.,

$$Cos(\alpha_{ij}) = \frac{\vec{\varepsilon_i} \cdot \vec{k_j}}{|\vec{\varepsilon_i}||\vec{k_j}|} \tag{2.21}$$

Since, the momenta of the three annihilation photons are ordered in energy, $|\vec{k_1}| > |\vec{k_2}| > |\vec{k_3}|$, three independent operators can be constructed to measure,

$$Cos(\alpha_{12}) = \frac{\vec{\varepsilon_1} \cdot \vec{k_2}}{|\vec{\varepsilon_1}||\vec{k_2}|};\ Cos(\alpha_{23}) = \frac{\vec{\varepsilon_2} \cdot \vec{k_3}}{|\vec{\varepsilon_2}||\vec{k_3}|};\ Cos(\alpha_{31}) = \frac{\vec{\varepsilon_3} \cdot \vec{k_1}}{|\vec{\varepsilon_3}||\vec{k_1}|}; \tag{2.22}$$

and thereafter combined together to have increased statistical precision. Therefore, this experimental methodology requires the reconstruction of decay events as described below,

$$o - Ps \rightarrow 3\gamma + \gamma', \tag{2.23}$$

where, γ denotes the primary annihilation photons and γ' denotes a secondary scattered photon belonging to any one of the three primary annihilation photons. While most of the previous experiments [27, 28] concentrated on measuring the

Table 2.2: Discrete symmetry odd-operator using linear polarization ($\vec{\varepsilon_i}$) and momentum ($\vec{k_j}$) directions of the annihilation photons from the decay of o-Ps$\rightarrow 3\gamma$, where i$\neq$j

Operator	**C**	**P**	**T**	**CP**	**CPT**
$\vec{\varepsilon_i} \cdot \vec{k_j}$	+	−	−	−	+

asymmetry of a given angular correlation, this study proposes to measure the expectation value over the entire region of its definition as a measure of the observed asymmetry [1].

CHAPTER3

JAGIELLONIAN-POSITRON EMISSION TOMOGRAPH (J-PET)

3.1 The J-PET Detector Properties

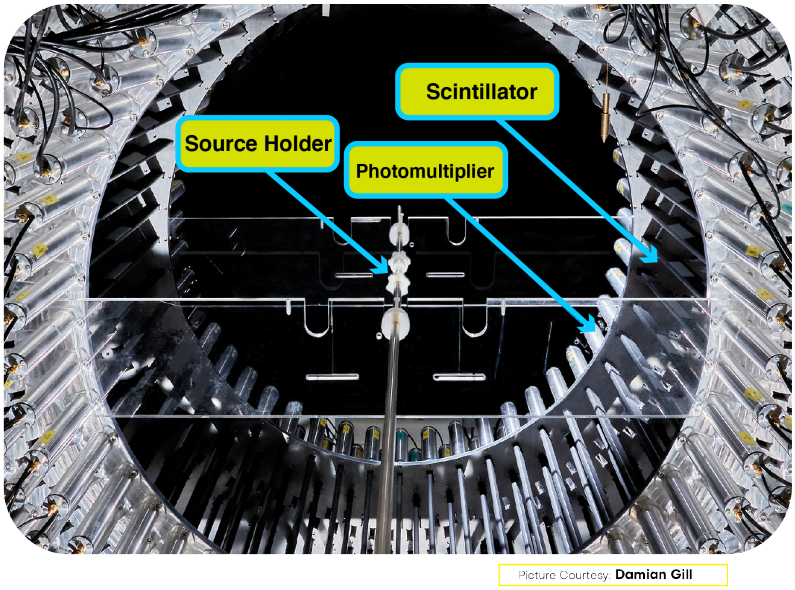

Figure 3.1: Front view of the J-PET detector where, the black strips are the scintillators wrapped in light protective foil. The silver tubes are housings of photomultipliers which are connected at either ends of the scintillator. The plastic source holder (white cylinder) at the center of the detector is the setup for the production of ortho-Positronium as part of this study.

Positron emission tomography (PET) is a non-invasive technique used in the diagnosis of various types of tumors at the cellular level [71]. All commercially available PET-scanners utilize relatively expensive crystal detectors for the

detection of annihilation photons [72–74]. The Jagiellonian - Positron Emission Tomograph (J-PET) is the first PET-scanner constructed using plastic scintilltor strips making it cost effective [5, 64, 67, 75]. One of the unique features of the J-PET detector is its ability to measure polarization of the annihilation photons [1, 6]. The J-PET detector consists of 192 plastic scintillator strips (EJ-230) of dimensions $500 \times 19 \times 7\ mm^3$ each, forming three concentric layers (48 modules on radius 425 mm, 48 modules on radius 467.5 mm and 96 modules on radius 575 mm) (Fig. 3.1) [5]. Each scintillator in the J-PET scanner is optically connected at two ends to photomultipliers as shown in Figure 3.1. Gamma quanta from Positronium annihilation interact with plastic scintillator strips, and cause emission of photons from the visible light spectrum. The optical signal from the sctintillator is read out at both of its ends by the photomultipliers (PMT) in the J-PET detector. In order to decrease photon losses the sides along a scintillator strip are covered with reflective foil. Polymers absorb internally less light emitted by scintillation from radiation than crystals, therefore the usage of longer polymer scintillator strips is possible [76]. The J-PET collaboration has created a J-PET analysis framework [77], which is a versatile, ROOT-based software [78] package that helps in tomograph reconstruction and calibration. The J-PET framework [77] serves as a foundation for analyzing the data and producing the findings provided in this thesis. The J-PET detector, together with the trigger-less Data Acquisition System (DAQ) constitutes an efficient photon detector with high timing properties [5]. This allows us to investigate the fundamental discrete symmetries in the purely leptonic sector [1].

3.2 Data Acquisition System

An advantage of the plastic scintillators over commonly used crystals is their lower price and shorter duration of signals (about 5 ns compared to 45 ns for LYSO crystal) [67]. This allows to use high activity sources and fast digital electronics readout. The J-PET Data Acquisition System is build out of Trigger Readout Board hardware equipped with Time-to-Digital Converters (TDC) and Field Programmable Gate Array (FGPA) devices for the TDC readout and data transmission [79]. Each analog signal from the PMT is sampled in the voltage domain at four thresholds [80]. This gives 4 points on the leading edge and 4 points at the trailing edge of the signal. A scheme of the registration process is shown on the left panel of Figure 3.2. Signals are probed at four thresholds, allowing the original signal form to be reconstructed [81]. Therefore, for a single photon interaction, the charge is estimated as a sum of Time Over Threshold (TOT) [77, 82] values measured for all thresholds at both sides of

scintillator given by,

$$TOT = TOT_A + TOT_B,$$

where,

$$TOT_{A,B} = \frac{thr_1}{thr_4 - thr_3} TOT_1^{A,B} + \frac{thr_2 - thr_1}{thr_4 - thr_3} TOT_2^{A,B} + \frac{thr_3 - thr_2}{thr_4 - thr_3} TOT_3^{A,B} + \frac{thr_4 - thr_3}{thr_4 - thr_3} TOT_4^{A,B},$$

where, $thr_4 - thr_3$ is used as the normalization factor. Continuous data collection (in a trigger-less mode) ensures that the recorded information is preserved and stored for high-level processing by specialised analysis tools [77]. From the time of scintillation light registration in photomultipliers at the ends

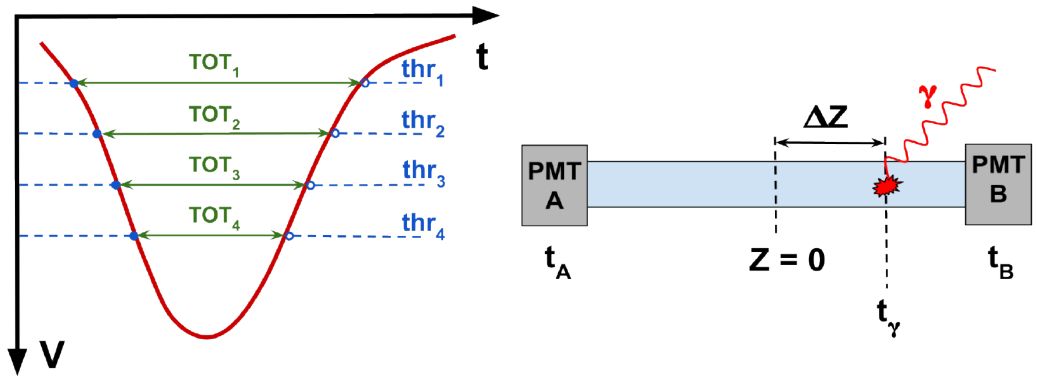

Figure 3.2: Left: Four voltage threshold levels are applied from the recorded signal (blue lines). Recorded times at both PMT's (t_A and t_B) are used for determination the gamma quantum interaction time (t_{Hit}) and place (Z_{Hit}) along the scintillator strip. The value of deposited energy corresponds to the sum of registered times over threshold (TOT) for all thresholds crossed by the signal. Right: The incident gamma quantum (red) interacts with the detector strip, causing photons to be emitted, which are then detected by photomultipliers (PMT).

of a single plastic scintillator strip, the time and position of a gamma quantum interaction in a scintillator can be estimated (t_{Hit} and Z_{Hit}). The distance (Δ z) along the strip between its center and the hit position (Figure: 3.2) can be expressed as:

$$\Delta z = \frac{(t_A - t_B) \cdot v}{2}, \tag{3.1}$$

where, v is the effective light signal velocity in the plastic scintillator [83]. The time of interaction t_{Hit} is obtained from a sum of the light registration times

at sides A and B of the scintillator:

$$t_{\mathrm{Hit}} = \frac{(t_{\mathrm{A}} + t_{\mathrm{B}})}{2} - \frac{L}{2v}, \tag{3.2}$$

where, L is the length of scintillator strip.

Gamma quanta interact with polymer scintillators mainly via the Compton effect and the characteristic spectra of deposited energy are described with a differential cross section for scattering in a solid angle dΩ given by the Klein-Nishina formula [69]:

$$\frac{d\sigma}{d\Omega} = \frac{{r_0}^2}{2}\left(\frac{E'}{E}\right)^2\left[\frac{E'}{E} + \frac{E}{E'} - sin^2\phi\right] \tag{3.3}$$

where, r_0 is the classical electron radius, E and E' denote energies of the primary and scattered photon and ϕ is the planar angle between their momenta.

The total energy deposited by gamma quanta is correlated with the sum of TOTs at all thresholds crossed by the signals on both A and B sides of a scintillator [82].

3.3 Experimental Setup and Measurement with J-PET

The first measurement with the J-PET detector to test the discrete symmetry odd-operator discussed in Table 2.2 was carried out with a point-like source placed at the center of the detector geometry in a source holder made of PA6 (Polyamide) of density 1.14 g/cm^3 to provide very lower attenuation of gammas from the Positronium decay [84]. Figure 3.3 shows the photo (Left) and schematic view (Right) of the source holder. The source holder was shaped as a cylinder with a total diameter of 2 cm. In the center of the holder a β^+ source was placed in the form of ^{22}Na covered in XAD-4 porous polymer [85] (as presented in scheme of Figure 3.3). To enhance the production of ortho-Positronium atoms [85]. The positrons emitted from the ^{22}Na source, ($^{22}Na \rightarrow {}^{22}Ne^* + e^+ + \nu_{\mathrm{e}}$), interact with the electrons in the XAD-4 porous polymer producing ortho-Positronium (o-Ps) which predominantly decays into three photons due to charge conjugation symmetry conservation ($o\text{-}Ps \rightarrow 3\gamma$) [55, 86]. Meanwhile, the excited $^{22}Ne^*$ de-excites emitting gamma quantum with an energy of 1274 keV ($^{22}Ne^* \rightarrow {}^{22}Ne + \gamma_{(1274\ keV)}$). A vacuum system connected to the source holder ensured pressure at a level of $\sim$1.2 Pa inside its volume. The measurement was performed for 122 days, resulting in a total of almost 100 TB of collected raw data. Reduction

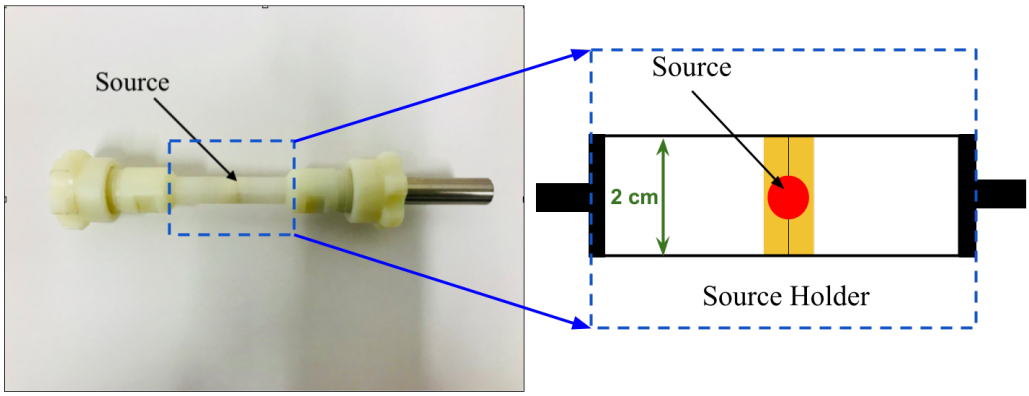

Figure 3.3: (Left) The real picture of the source holder. (Right) The schematic of the source holder with a point-like source (Red) covered with XAD-4 (Yellow) in the center.

of such a high data flux, resulting from the trigger-less mode of J-PET data acquisition requires stringent discrimination of background in order to allow for effective analysis of the J-PET data [79]. The analysis of the data was performed using the J-PET Analysis Framework software [77,87]. The J-PET data reconstruction is a multi-stage process based on a dedicated analysis software, the J-PET Analysis Framework [88]. It is developed in a C++ programming language and is based on the Open Source library ROOT [78]. The source code of the project is available on the GitHub service under the Apache Licence [87]. The analysis of data with the J-PET Framework consists of several modules. Each of them corresponds to a particular computing task e.g. calibration procedure or reconstruction algorithm. This approach allows the user to choose between available reconstruction algorithms or create a dedicated analysis module and easily implement it into the data processing chain. This research experiment was modeled in the Monte Carlo simulation package called J-PET-Geant4 [89]. The program is based on the Geant4 [90] simulation package, which controls the tracking of particles through detector geometry and uses well tested routines to simulate interactions. At the first stages of data reconstruction, single times recorded at certain voltage thresholds applied to the PMT electric signals were assembled into representations of these signals as presented in Figure 3.2. For each signal, the time over threshold (TOT) value was calculated using information on all available thresholds. Subsequently, pairs of signals (referred to as hits in the further considerations) coming from the same γ interaction were identified. Signals were paired if they originated from distinct sides of the same detection module (scintillator strip) and their arrival times (estimated using time at the leading edge on a threshold lowest in terms of absolute voltage) were separated

by no more than 5 ns [88]. The last stage of early reconstruction comprised assembling event candidates as sets of hits contained within a time window of 200 ns. Although such a time window is broad with respect to possible time differences in a physical event, its purpose was a reduction of data volume without limiting further fine selection of event candidates by more strict timing requirements. The experiment as part of this study was conducted through 2017-2020 in four parts as described in the Table 3.1.

Table 3.1: The table describes the four experimental-runs conducted by the J-PET collaboration for the test of P, T and CP symmetry using the discrete symmetry odd-operator described in Table 2.2.

Run	**Source Activity MBq**	**No. of o-Ps Candidates**	**% of the Total**	**# of Days**
R 1	5.0	47 597	5.9	6
R 2	5.0	313 563	41.8	30
R 3	1.0	251 257	34.8	46
R 4	1.0	157 277	16.2	40

The first column of Table 3.1 describes the subsequent names of the experimental runs as R1, R2, R3 and R4. The first two experimental runs (R1 and R2) were conducted with a source activity of 5 MBq. Similarly, the next two experimental runs (R3 and R4) were conducted with a 1 MBq source activity.

3.3.1 Auxiliary Test Experiments

In the beginning of 2017, before conducting the experiments illustrated in the previous section, two test measurements with the J-PET detector was conducted with a point-like source using a metallic source holder as shown in Figure 3.4. The details of the two test experiments is described Table 3.2.

Table 3.2: The table describes the two test experimental-runs conducted using the metallic source holder.

Run	**Source Activity MBq**	**No. of o-Ps Candidates**	**% of the Run**	**# of Days**
T 1	1.0	21 974	2.8	3
T 2	10.0	18 973	2.4	60

The two test experiments, T1 was measured for 3 days with a source activity of 1 MBq and T2 was conducted for 60 days using source activity of 10 MBq.

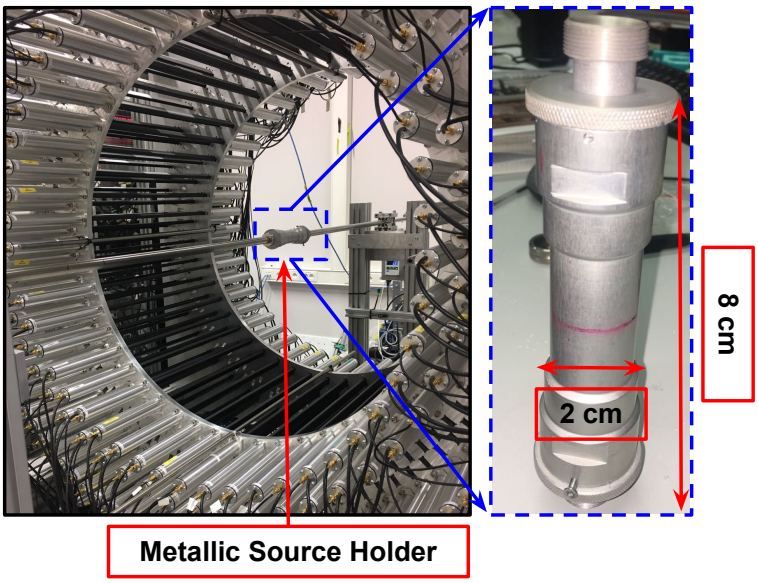

Figure 3.4: (Left) The real picture of the source holder placed inside J-PET detector. (Right) Individual photo of the source holder.

The measurement setup was similar to the experimental setup described in the previous section, however a point-like ^{22}Na source was placed in the center of the metallic source holder made of stainless steel of density 7.5 g/cm^3. The β emitting source was covered in XAD-4 porous polymer to aid the production of ortho-Positronium. Due to the high density of the metallic source holder, the measurement indicated noisy reconstruction of signal events due to the attenuation of photons within the metallic source holder. Therefore, the two test experiments acquired o-Ps signal candidates accounting to only $\sim$5% of the total sample and was used only as a test data. In addition, one experimental run was conducted without a radioactive source in order to gather pure cosmic ray events for estimations of one of the background sources as is described is Section 4.1.1.

CHAPTER4

SIGNAL SELECTION AND EXPERIMENTAL CONDITIONS

4.1 Segregation of o-Ps$\rightarrow 3\gamma+\gamma'$ events

Determining the momentum direction of the annihilation photon of the decaying ortho-positronia is required to calculate the angular correlation operator outlined in Table 2.2. As a reminder, the schematic representation in Figure 4.1 shows one of the orientation of a signal event favourable for this study. The preselection of data only required presence of at least four γ interactions (*hits*) in a time window of 200 ns. A set of hits contained within such a time window will be later on referred to as an *event*.

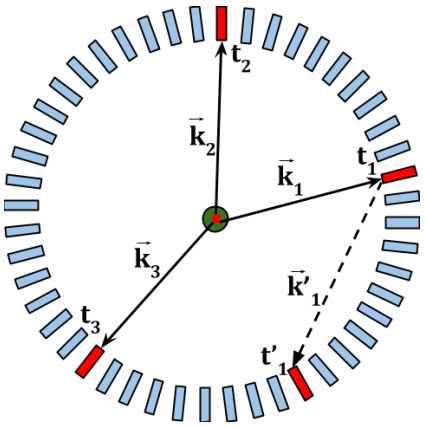

Figure 4.1: Schematic of a single layer of the J-PET detector. A point-like positron source (red) placed in the center covered in XAD-4 porous polymer (green). The superimposed arrows indicate gamma photon originating from the annihilation photons from ortho-positronium decay (k_1, k_2 and k_3) and secondary scattered photon (k_1'). The photon interaction time is denoted as t_1, t_2, t_3 and t_1', respectively.

Hit multiplicity of identified annihilation photon candidates observed in a single event is presented in Figure 4.2. The requirement of at least four hits in one event reduces the measured experimental data sample by a factor of 10^3, as

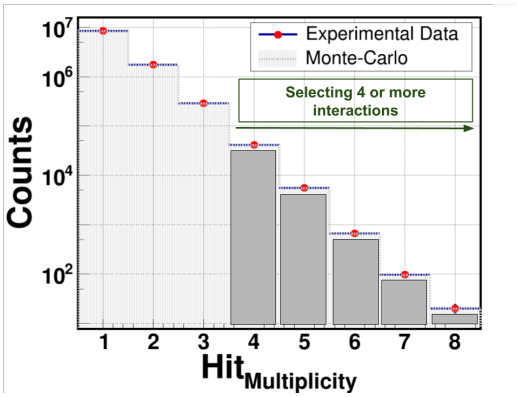

Figure 4.2: The distribution of number of photon interactions (hits) recorded within each event ($Hit_{Multiplicity}$).

in Figure 4.2. The active scintillating region along the axial direction of strips is constraint to a length of 46 cm to reduce scatters from aluminum frames of the detector, variations of attenuation length and resolution effects at the end of scintillator strips. Therefore, the interaction position of each hit along the Z-axis is restricted in this analysis as:

$$|Z_{Hit}| \leq 23cm, \tag{4.1}$$

shown in Figure 4.3 with a signal loss of 9.5%.

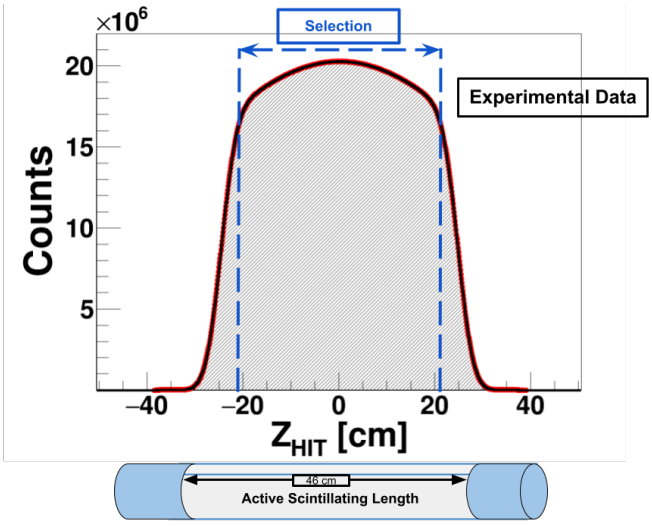

Figure 4.3: Distribution of the hit interaction position along the axial direction with a schematic indicating the active scintillating region in a single J-PET detector module.

Cosmic radiation is an inevitable background contribution to the experimental measurement with the J-PET detector. It is important to estimate and reject the significant contribution of the cosmic radiation interactions within the J-PET detector in order to improve the sensitivity while testing discrete symmetries. Cosmic radiation are uniquely segregated from the data sample due to their large energy deposits in the detector. For which two experimental test runs were conducted: one without the placement of any radioactive source in the vicinity of the J-PET detector in order to study the cosmic radiation contribution to the experiment, and the other experimental run was conducted by placing a point-like ^{22}Na source in the center of the detector geometry. The J-PET detector measures the energy deposition of the interacting photons as the Time over Threshold (TOT).

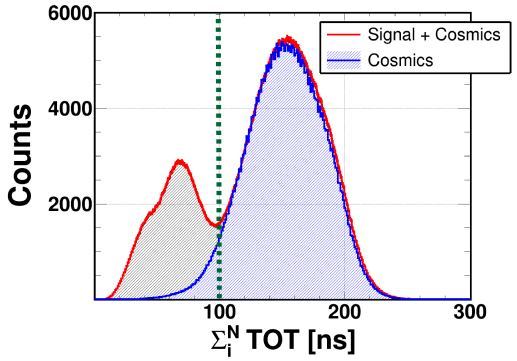

Figure 4.4: Experimental distribution of time-over-threshold (TOT) for measurement with (red) and without (blue) positronium source. The green dashed line indicates the possible separation of annihilation photons from cosmic radiation.

Figure 4.4 shows the sum of TOT for four-interactions in an event time window: 200 ns. The green dashed line indicates the possible separation of events with $\Sigma_i^N\ TOT$ above 100 ns which can reduce the registered cosmic radiation by 97.5% [30]. To increase the effectiveness of rejecting both de-excitation photons and cosmic radiation, the selection criteria on the TOT for each photon separately is applied as presented in Figure 4.5. The TOT distribution can also distinguishes the Compton edge corresponding to the registered annihilation photons (between 20 ns to 28 ns) and the de-excitation photons (greater than 28 ns). By placing a selection criteria on the TOT for each hit as:

$$TOT(Hit) \leq 17ns, \tag{4.2}$$

we suppress the background by 47.5% with a signal efficiency of 93.5%.

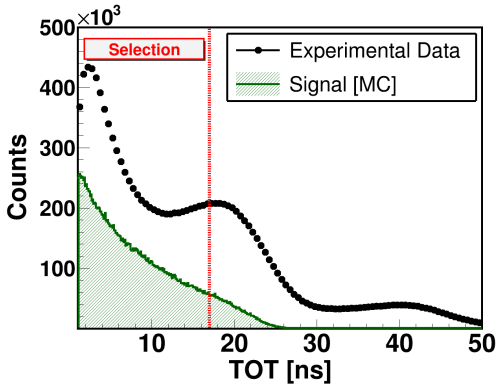

Figure 4.5: Energy deposited by interacting photons in the plastic scintillators as a function of the Time over Threshold.

4.1.1 Selection of Primary Annihilation Photons (3γ)

For each of the three interacting primary annihilation photon candidates (i = 1, 2 and 3), we measure the following physical quantities: Cartesian coordinates of the interaction position (X_i, Y_i, Z_i), and time of photon interaction (t_{Hit_i}). The source position (S_x, S_y, S_z) was reconstructed for every 24 seconds of measurement from back-to-back p-Ps$\rightarrow 2\gamma$ events. Thereafter, the emission time of each of the three photons is calculated as follows:

$$ET_i = t_{Hit\,i} - \frac{d_i}{c} \tag{4.3}$$

where,

$$d_i = \sqrt{(X_i - S_x)^2 + (Y_i - S_y)^2 + (Z_i - S_z)^2} \tag{4.4}$$

is the distance between the photon interaction and the source position, and c denotes the speed of light. Then the Emission Time Spread (t_{ETS}) of a three-photon interaction is calculated as follows:

$$t_{ETS} = ET_3 - ET_1, \tag{4.5}$$

where, the calculated emission times are ordered such that ($ET_1 < ET_2 < ET_3$), respectively. The distribution of t_{ETS} is shown in Figure 4.6. The selection criteria,

$$t_{ETS} \leq 1.4ns, \tag{4.6}$$

allows to select primary photons from the same annihilation event within the co-incident event-time window.

Since the experiment was conducted by placing a point-like β^+, the distance of the annihilation plane for true o-Ps signal candidates must be close to the source position (S_x, S_y, S_z). The interaction positions (X_i, Y_i, Z_i) for the primary

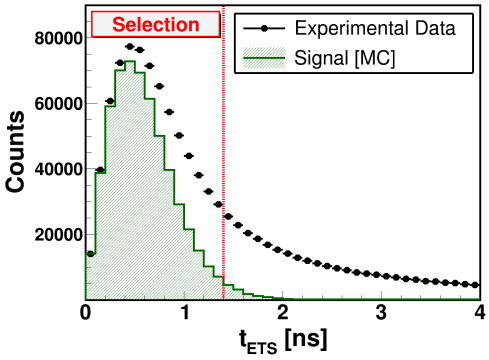

Figure 4.6: Emission Time Spread (t_{ETS}) distribution.

annihilation photon candidates (i = 1, 2 and 3) can be used to construct the annihilation plane. The equation of the annihilation plane is given as,

$$Ax + By + Cz + D = 0$$

from which we calculate the distance of the annihilation plane to the source position,

$$DOP = \frac{|A.S_x + B.S_y + C.S_z + D|}{\sqrt{A^2 + B^2 + C^2}}$$

The selection criteria,

$$DOP \leq 4cm, \tag{4.7}$$

is applied in the analysis to suppress the background by $\sim$81%. The distribution of DOP is shown in Figure 4.7.

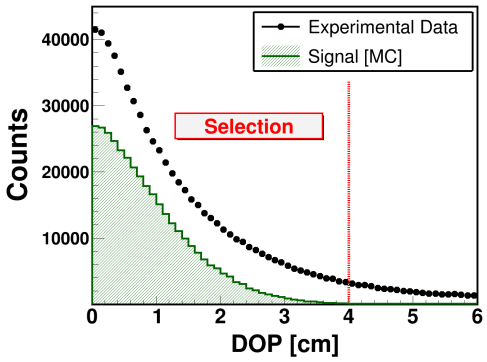

Figure 4.7: Distance of the annihilation plane (DOP) distribution.

The next stage of the data analysis requires the selection of the primary annihilation photons from the decay of o-Ps$\rightarrow 3\gamma$. Using kinematic properties of

the o-Ps bound system and favourable features of the J-PET detector, the following selection criteria were formulated.

One of the key features of the J-PET detector is its fast timing properties from plastic scintillators [3, 4] which allows the calculation of the relative azimuthal angles between the interacting photons.

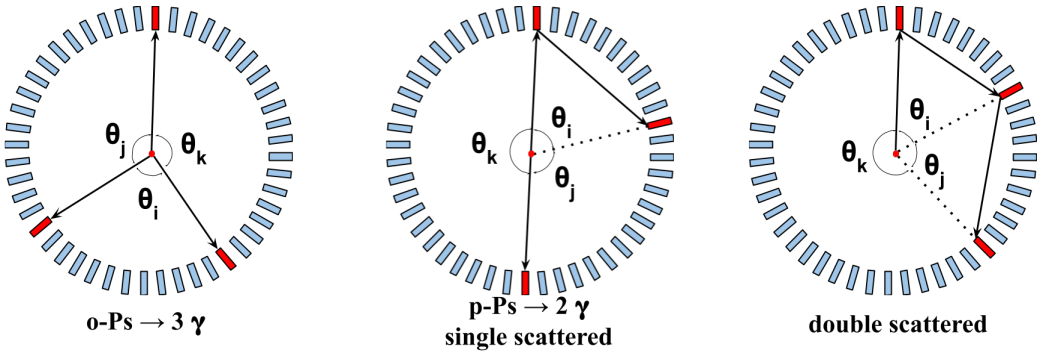

Figure 4.8: Illustration of the possible response of the detector to o-Ps$\rightarrow 3\gamma$ and p-Ps$\rightarrow 2\gamma$. The blue ring represents a single layer of the J-PET detector. The red color indicates strips where the gamma quanta were registered. The solid arrows represents gamma quanta occurring in the event, while dotted lines indicate reconstructed gamma quanta under the assumption of o-Ps$\rightarrow 3\gamma$.

Figure 4.9 shows the distribution of $\theta_i + \theta_j$ vs $\theta_i - \theta_j$, where $\theta_{i,j,k}$ are the ordered opening angles ($\theta_i < \theta_j < \theta_k$) between registered photons. For the $o-Ps \rightarrow 3\gamma$ process, due to the momentum conservation, $\theta_j > 180^\circ - \theta_i$ and therefore events corresponding to the $o-Ps \rightarrow 3\gamma$ decay will be beyond the 180° on the X-axis. Background events can be inferred from the middle and left panel of Figure 4.8. The spectra on the top-left panel of Figure 4.9 shows the distribution of sum and difference of the azimuthal angle for three interacting photons, probable candidates of o-Ps primary annihilation photons. The enhancement of events above 180° on the X-axis of Figure 4.9, corresponds to the existence of the decay of o-$Ps\rightarrow 3\gamma$ in the measured data sample [91]. The selection criteria in Equation 4.8 suppresses the background by 97%,

$$\theta_i + \theta_j \geq 190^\circ. \tag{4.8}$$

In order to validate the existence of o-Ps signal events in the final data sample the decay time of the produced positronium is calculated. The difference of emission time of the de-excitation photon and an average emission time of the three annihilation photons as shown in the right panel of Figure 4.10. The de-excitation photon is selected solely based on the TOT for a selected hit apart from the selected three primary annihilation photons. The spectrum shows a

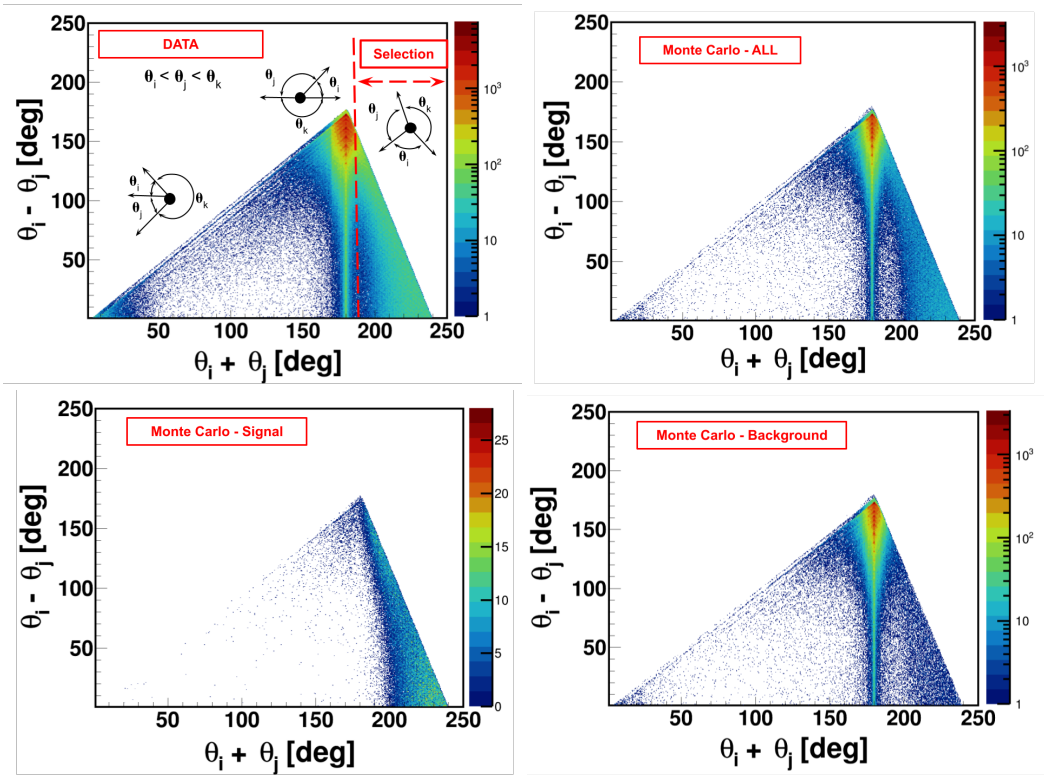

Figure 4.9: The figure above shows the relation between the sum $(\theta_i + \theta_j)$ and difference $(\theta_i - \theta_j)$ of two smallest relative azimuthal angles for three interacting photons in the Experimental Data, Reconstructed Monte Carlo All, Background and Signal, respectively. Distribution of $o\text{-}Ps \rightarrow 3\gamma$ lies as part of the enhancing events beyond 180° on the X-axis. Events with two photons from p-Ps $\rightarrow 2\gamma$ annihilation and one of them scattering and registering in the detector, lies at the prominent band at 180° (on the X-axis). Events where one gamma is missing detection and the other undergoes two scatterings within the detector are spread over the 180° band on the X-axis.

sharp maximum corresponding to the annihilation of para-Positronium and direct $e+e-$ annihilations. The long tail corresponds to the decays of ortho-Positronium atoms. This distribution was constructed after the selection criteria in equation 4.8 for the purpose of validating the selection criteria of the primary annihilation photons [32].

4.1.2 Selection of Secondary Scattered Photon (γ')

The final stage of the analysis requires to identify a secondary scattered annihilation photon (γ') and thereafter reconstruct the momentum direction, for

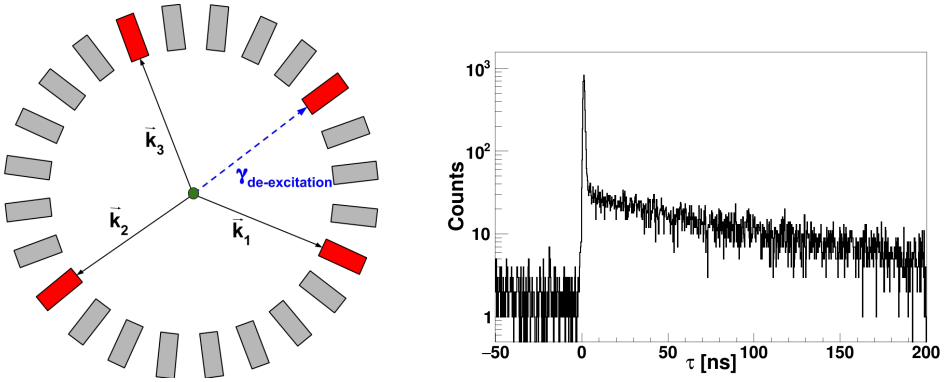

Figure 4.10: (Left) Schematic of the J-PET scanner registering the de-excitation photon ($\gamma_{de-excitation}$) represented using dashed blue line and three primary annihilation photons ($|\vec{k}_1| > |\vec{k}_2| > |\vec{k}_3|$).
(Right) Positronium decay time (τ) distribution in the XAD-4 porous polymer, obtained from the measurement with the J-PET detector. The decay time distribution is obtained by identifying and time stamping the de-excitation photon and the corresponding three annihilation photons from the decay of ortho-Positronium.

example, $\vec{k}_1'$ as shown in Figure 4.1, of the secondary scattered photon to construct the symmetry-odd operator as described in Table 2.2.

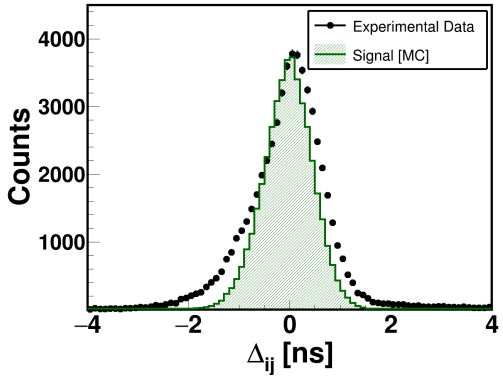

Figure 4.11: Distribution of Δ_{ij} as described in the text.

As the next step, in order to assign the scattered photon to its corresponding parent-primary annihilation photon, the difference of the time variable is calculated as,

$$\Delta_{ij} = (\delta_{ij} - d_{ij}/c) \tag{4.9}$$

where,

$$\delta_{ij} = t_i - t_j \tag{4.10}$$

i.e., the difference in time of interactions, d_{ij} represents the distance between the two interactions and c is the speed of light. Where, i = 1, 2, 3 (o-Ps annihilation photons) and j = 1,...($Hit_{Multiplicity}$ - 3). Thus, Δ_{ij} should be equal to zero in case if the j^{th} interaction is due to the i^{th} primary annihilation photon. Therefore, j^{th} hit is assigned to this i^{th} primary photon for which Δ_{ij} is smallest.

Henceforth, the vector ($\vec{\varepsilon}_i$) as part of the symmetry-odd operator mentioned in Table 2.2 is estimated as the cross-product of the momentum direction of the primary and secondary scattered annihilation photons ($\vec{k}_i \times \vec{k}_i'$) [1, 29]. This iterative algorithm was applied to select the secondary scattered photon and correlated to the parent primary photon with a selection efficiency of 99%.

4.2 Normalization of Monte Carlo to Experimental Data

After selection criteria for signal candidates are established, the Monte Carlo parameters, equivalent to the experimental resolutions (σ_t - hit time smearing and σ_Z - smearing of hit position along the scintillator strip) and measurement condition (E_{th}, lowest threshold in energy units) were optimized by improvement of Monte Carlo to Experimental Data agreement and the whole analysis was redone afterwards. The positronium decays were generated by the GEANT4-based program [90].

Table 4.1: Table summarizes the scan of smearing parameters applied to the reconstructed Monte Carlo simulations.

Smearing	**Range of the Scan**	**Applied Value**
σ_t	125 to 350 [ps]	225 [ps]
σ_Z	0.97 to 5.0 [cm]	2.5 [cm]
E_{th}	28 to 35 keV	31.25 [keV]

The program itself contains the implementation of the whole geometry of the J-PET detector setup [87]. It takes into account also known physical processes like Compton scattering [69] and other photon interactions in the detector material, as well as the detector and target properties established and described in Chapter 3, like: position of the source, size and position of the source holder and spread of the decay events within the detector acceptance. Afterwards a given property (t,

Z_{Hit} and E_{th}) of hits in the event were smeared and reconstructed in the same way as the experimental data. Finally the Monte Carlo signal and background were fit to the experimental data with normalization as a free parameter.

The obtained spectra were compared to the experimental ones via calculating the χ^2 derived from the maximum likelihood method. The determination of the smearing parameters was based on the simultaneous comparison of all experimental angle spectra with the reconstructed Monte Carlo as shown in Table 4.12. Please note that the energy smearing is kept constant with respect to the energy deposition of the photon. Furthermore, keeping the smearing constant as described in Table 4.1, the reconstructed Monte Carlo events are normalized to fit the experimental data with maximum likelihood which is described in the next section.

4.2.1 Minimization: Maximum-Likelihood Fit

In the Monte Carlo sample, apart from the signal and non-signal (background) events, the sample of wrongly reconstructed signal events was identified (mis-reconstructed signal), for example ortho-Positronium annihilation into three photons, but with some hits not correctly assigned as annihilation photons.

As described in Section 4.1.2, the distribution of the sum and difference of the two smallest angles in three-photon interactions (θ_i and θ_j) describes the signal and background candidates distinctly well. Therefore for the maximum likelihood fit, the distribution of the sum of the two smallest relative azimuthal angle is used. The maximum likelihood fit is performed based on the χ^2 function using the software library TMinuit [92] as described:

$$\chi^2 = \Sigma_{i=1}^{Bins} \frac{(N_i^{DATA} - N_i^{MC})^2}{\sigma^2} \tag{4.11}$$

where, N_i^{DATA} is the i^{th} bin content of the experimental data, N_i^{MC} is the i^{th} bin content of the total Monte Carlo. The total Monte Carlo has three components, the signal (green histogram in Figure 4.13) scaled by a factor A, mis-reconstructed signal (pink histogram in Figure 4.13) also scaled by a factor A, and the background (blue histogram in Figure 4.13) scaled by a factor B. Therefore, the χ^2 function for the fit is computed with two free parameters A and B, such that the total Monte Carlo is,

$$N_i^{MC} = A \cdot N_i^{Signal} + A \cdot N_i^{Mis-Reconstructed\ Signal} + B \cdot N_i^{Background} \tag{4.12}$$

and the square of the total error given by

$$\sigma^2 = (N_i^{DATA} + A^2 \cdot (N_i^{Signal} + N_i^{Mis-Reconstructed\ Signal}) + B^2 \cdot N_i^{Background}). \tag{4.13}$$

The illustration of the minimization and fit is shown for the four parts of

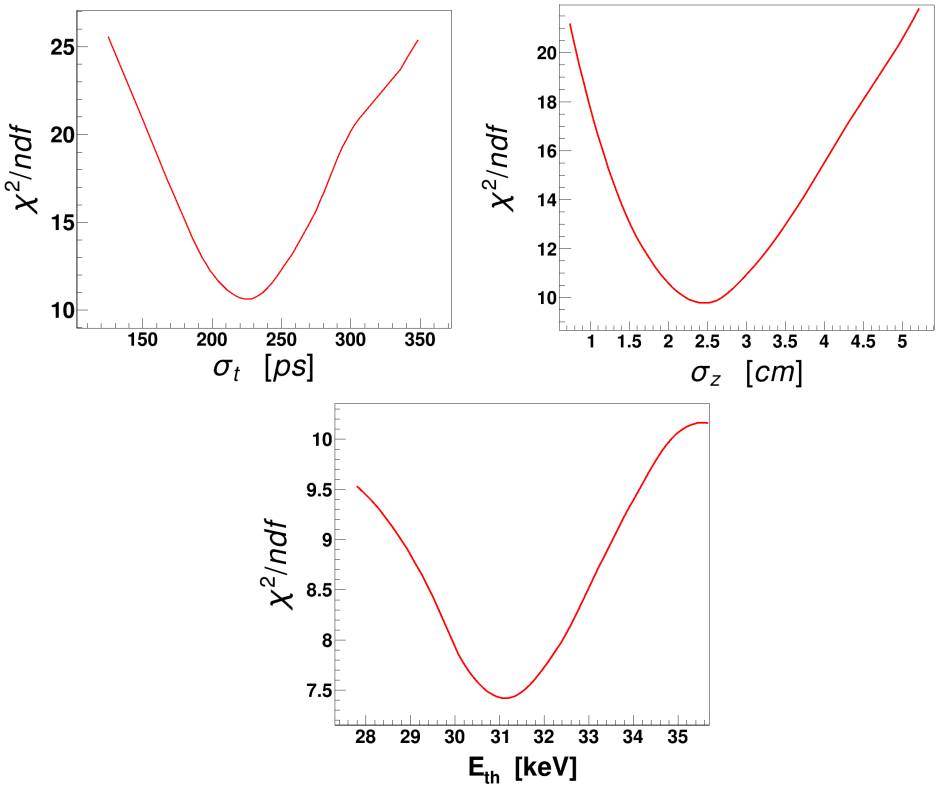

Figure 4.12: χ^2/ndf obtained from the comparison of simulated and experimental data by means of the maximum likelihood. (Top-Left) χ^2/ndf as a function of time-smearing parameter (σ_t), the minimum χ^2/ndf value corresponds to 225 ps. (Top-Right) χ^2/ndf as a function of Z-smearing parameter (σ_Z), the minimum χ^2/ndf value corresponds to 2.5 cm. (Bottom-Center) χ^2/ndf as a function of energy threshold (E_{th}) parameter, the minimum χ^2/ndf value corresponds to 31.25 keV.

the experiment in Figure 4.13, where, the red solid line is total Monte Carlo

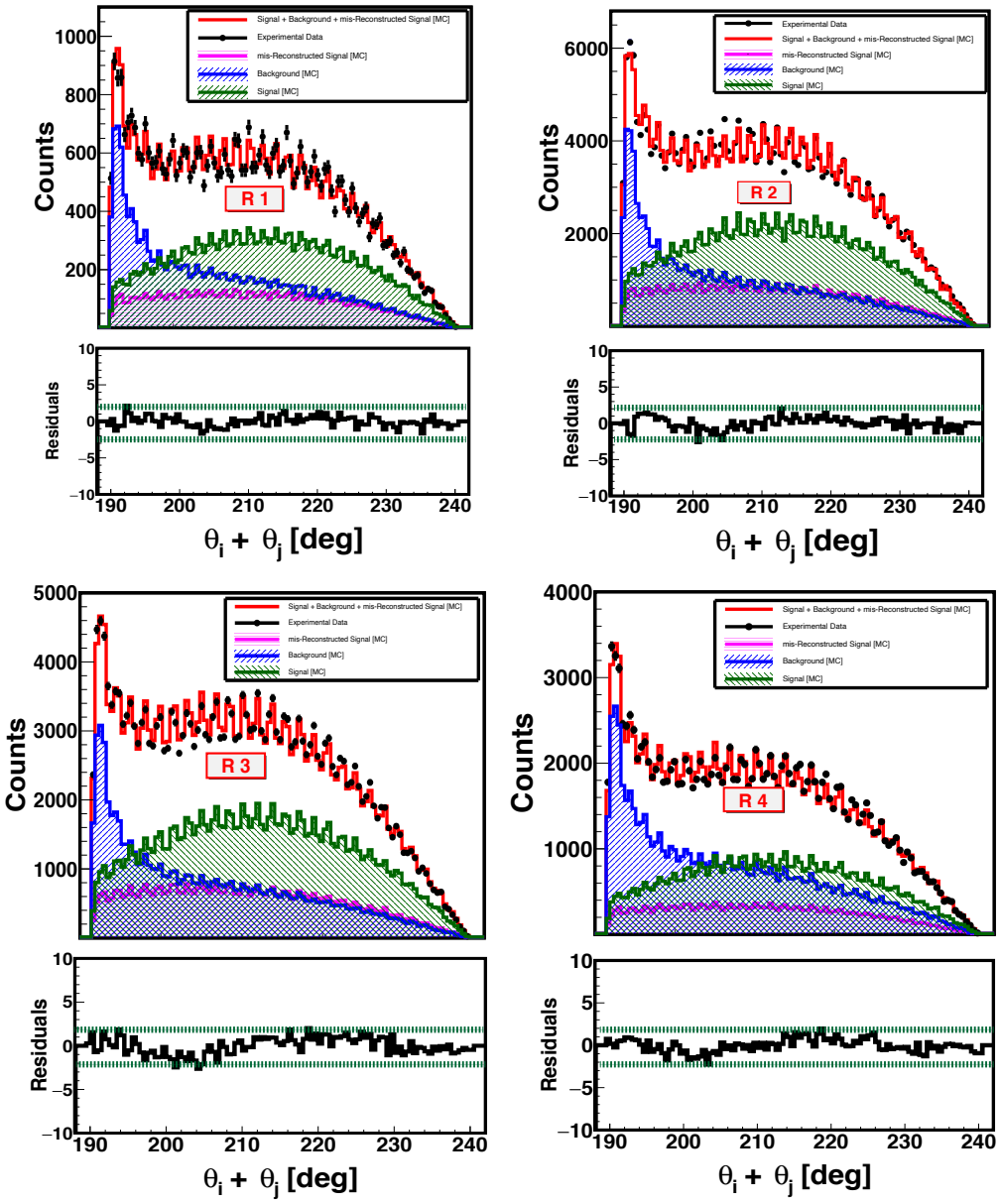

Figure 4.13: The Monte Carlo Signal and Background is fit to the Experimental Data on the projection of the sum ($\theta_i + \theta_j$) of the two smallest azimuthal angles between the 3γ of o-Ps decay distribution. Green dashed lines at residual plots indicate $\pm 2\sigma$ region. The fit was performed for each experimental run (R 1, R 2, R 3, R 4), separately.

minimized and scaled to the experimental data points denoted by the black solid circle points. The spectra on the bottom row in Figure 4.13 presents residual errors of the fits for the normalized histogram calculated as,

$$Residual_i = \frac{(N_i^{DATA} - N_i^{MC})}{\sigma}. \tag{4.14}$$

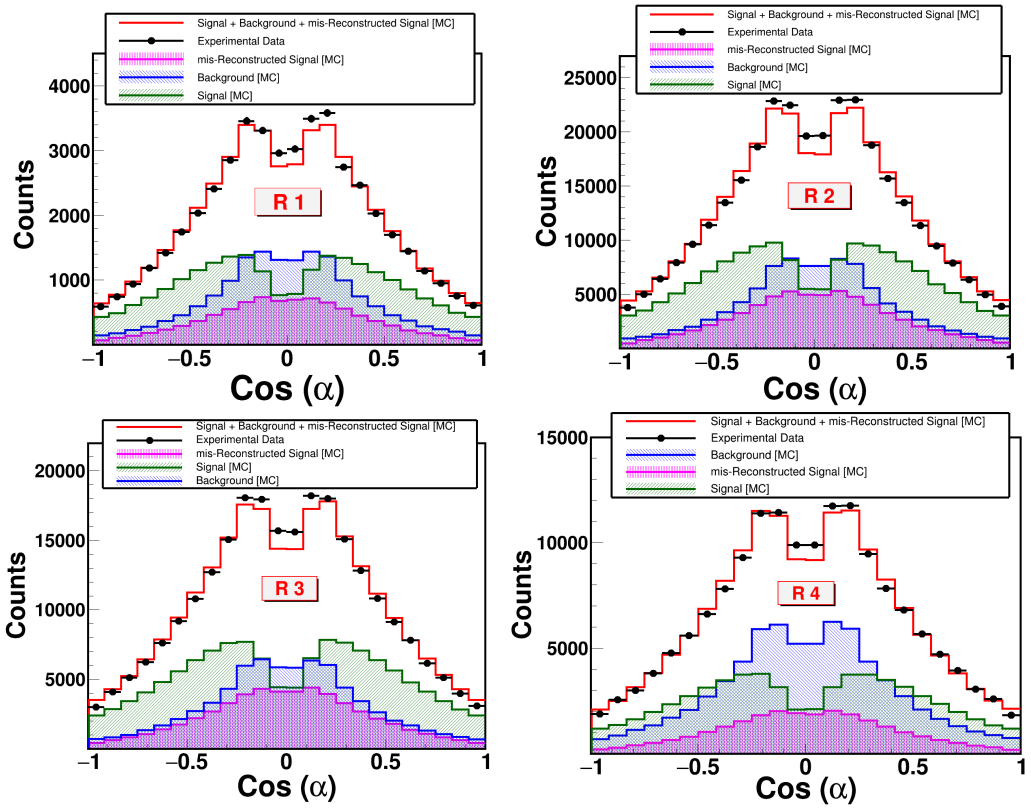

Figure 4.14: The Monte Carlo Signal and Background with Experimental Data on the Cos(α) distribution using scaling factors derived from Table 4.2

The Table 4.2 summarises the scaling factors for signal and mis-reconstructed signal as A and background as B, respectively, from the fit for each part of the experimental measurement, where, number of degrees of freedom, ndf = 101. Different values of scaling parameters for different runs are due to the different sizes of the MC samples generated.

Since the operator is constructed for the same data sample, the scaling factors from Table 4.2 obtained from the fit as shown in Figure 4.13 are applied to the histogram distribution of Cos(α) as described in Equation 2.21. Figure 4.14 shows the distribution of Cos(α) for the four parts of the experiments. The red solid histogram described the total Monte Carlo fit to the experimental data in black

Run No.	Scaling Factor A	Scaling Factor B
R 1	0.130 +/- 0.003	0.260 +/- 0.010
R 2	0.607 +/- 0.006	0.997 +/- 0.023
R 3	0.240 +/- 0.002	0.392 +/- 0.086
R 4	0.187+/- 0.003	0.652 +/- 0.014

Table 4.2: Scaling factors obtained from the fit for the signal and background components for each part of the experiment.

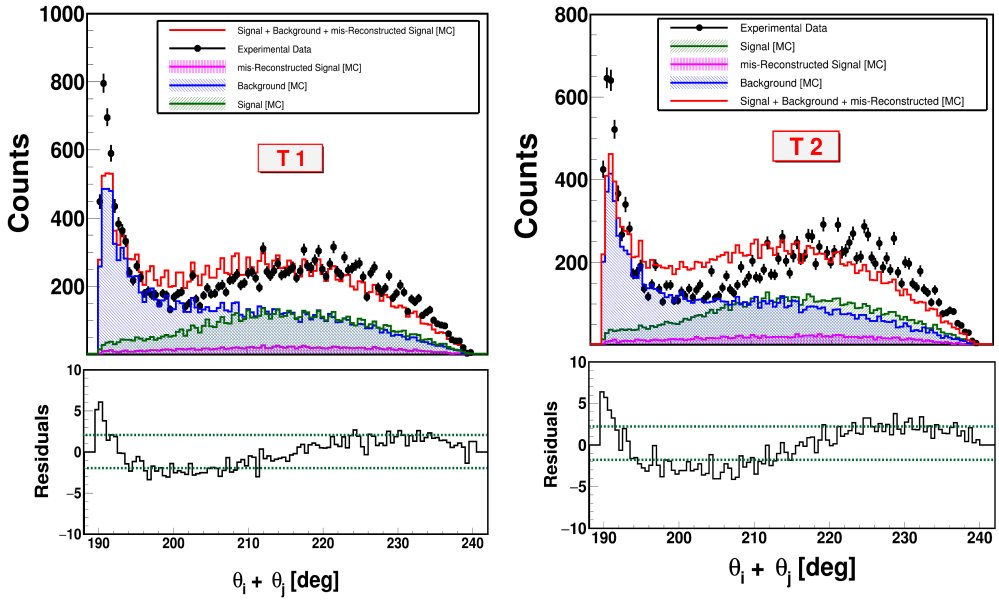

Figure 4.15: The reconstructed Monte Carlo fit to the experimental data for the two test measurements T 1 and T 2.

solid circle points. The signal and background events are shown in the green and blue histogram, respectively.

From the obtained results with agreement of the reconstructed Monte Carlo to the Experimental data, we deduce the purity and analysis efficiency, as described in Table 4.3.

4.2.1.1 Auxiliary Test Experiments

The illustration of the minimization and fit is shown for the two test experiments in Figure 4.15. Although the overall Monte Carlo to Experimental Data is vast

Run No.	Purity %	Efficiency %
R 1	48 ± 0.25	7 ± 0.08
R 2	50 ± 0.14	8 ± 0.05
R 3	50 ± 0.18	10 ± 0.06
R 4	40 ± 0.22	10 ± 0.04

Table 4.3: The purity and analysis efficiency of each part of the experimental measurement deduced from the reconstructed Monte Carlo through spectra shown in Figure 4.14

with respect to experimental runs R 1-4 (as listed in Table 3.1), the agreement is not that good in the data for T 1 and T 2 runs as expected due to the usage of metallic source holder (see Table 3.2).

4.2.2 Background Subtraction, Efficiency and Acceptance Correction

The Experimental data sample is further purified by subtracting the background component (true background and mis-reconstructed signal). Then the scaled background is subtracted from the total experimental data to have pure signal events. The obtained signal events are corrected for the analysis efficiency and the detector acceptance using the efficiency and acceptance maps, as shown in Figure 4.16.

The efficiency map (E) is calculated from the Monte Carlo as the ratio of the signal events after and before the analysis chain. The acceptance map for the entire data sample is shown in the bottom-right panel of Figure 4.16. Reconstruction of such events is possible only if all four gammas interact with the scintillators of the J-PET detector. The schematic of the signal event is depicted in the top-right panel of Figure 4.16. In reality the true signal event necessary to construct the symmetry odd-operator is $o-Ps \rightarrow 3\gamma$ with at least one photon interacting with the scintillator via compton scattering as shown in the bottom-left panel of Figure 4.16. Therefore, the acceptance map as shown in the bottom-right panel of Figure 4.16 is constructed as a ratio of detected o-Ps annihilation events with four interactions (3 primary annihilation photons and one secondary scattered photon) and the total number of produced o-Ps with at least one annihilation photon interacting with the detector as shown in the bottom left panel of Figure 4.16.

The final number of events in the i^{th} bin is therefore calculated as

$$N_i = \frac{DATA_i^{After\ Analysis} - A \cdot N_i^{MC\ Mis\ Reconstructed} - B \cdot N_i^{MC\ Background}}{\varepsilon_i^{Analysis} \cdot \varepsilon_i^{Acceptance}} \tag{4.15}$$

and the sum of all the four runs in presented in Figure 4.17 as a function of Cos(α).

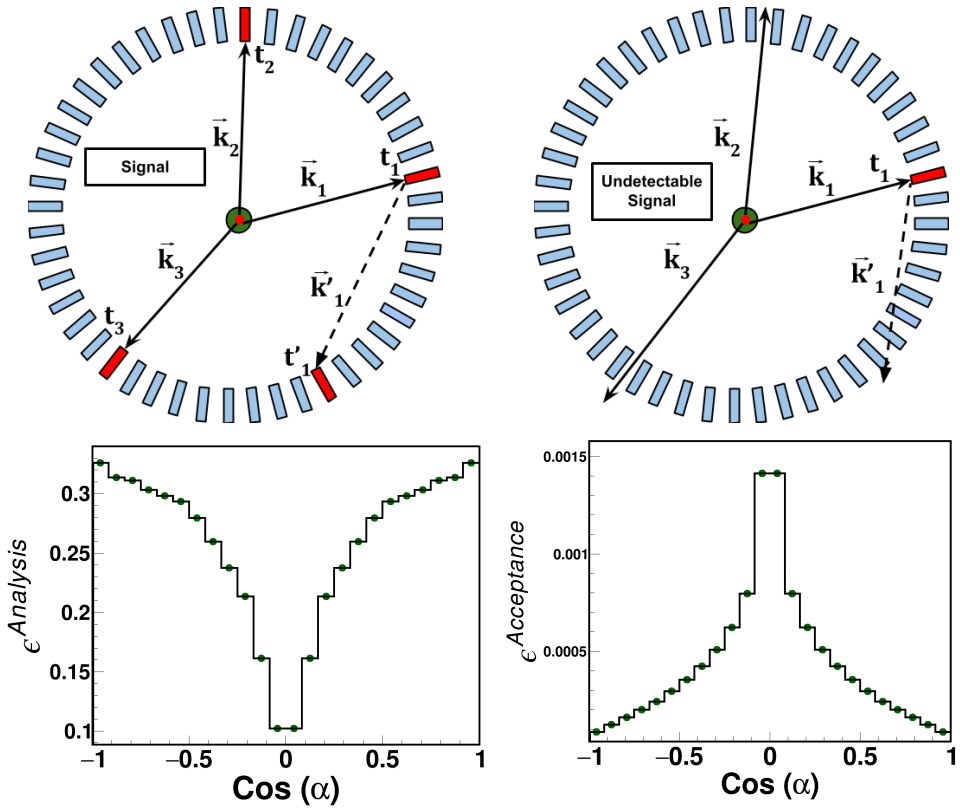

Figure 4.16: The figure shows the efficiency map on bottom-left panel and the schematic of the detector accepted signal event is shown on the top-left panel. The acceptance map is illustrated in the bottom-right panel with the schematic of an undetectable signal on the top-right panel.

4.3 Expectation Value of the Discrete Symmetry Odd-Operator

To derive the expectation value of the discrete symmetry odd-operator, the mean value of the Cos(α) distribution is calculated to infer the same. The expectation value and its error is computed for different parts of the measured experimental data as described in Table 4.4. Table 4.4 shows the weighted mean value of the Cos(α) distribution after the efficiency and acceptance correction, respectively. The final result is taken as the total weighted average of the expectation value derived from the four experimental measurements reported, i.e.,

$$< O >_{J-PET} = 0.0005 \pm 0.0007_{stat}. \tag{4.16}$$

Figure 4.18 visually represents the result obtained in Table 4.4.

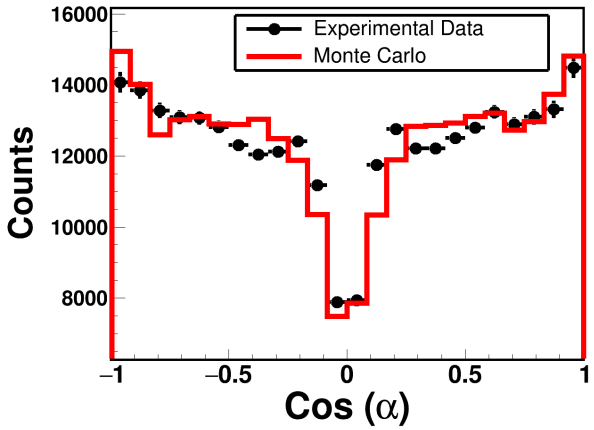

Figure 4.17: Experimental data (black points) after performing the signal efficiency correction and acceptance correction is compared with the true Monte Carlo (red solid line).

10^{-4}	**R 1**	**R 2**	**R 3**	**R 4**	Weighted Average
Expectation Value	-1 ± 79	-9 ± 36	10 ± 34	29 ± 56	**5.2 ± 6.7**

Table 4.4: Summary of the obtained expectation value result.

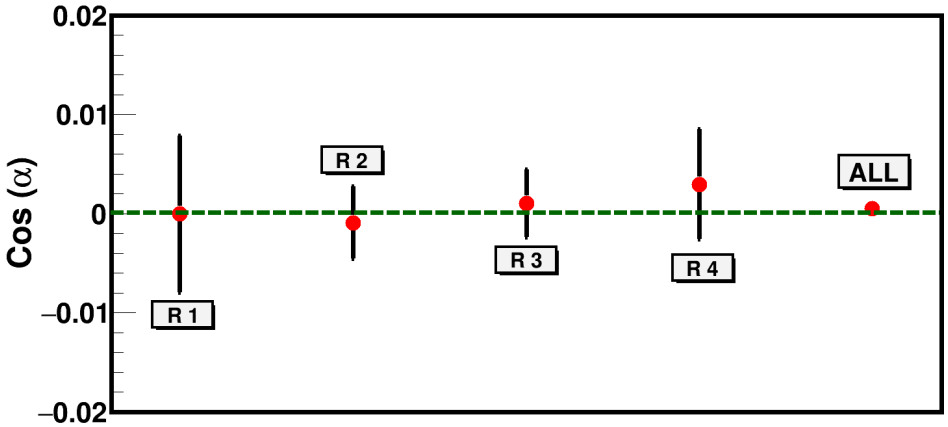

Figure 4.18: Visual representation of the expectation value of the discrete symmetry odd-operator with its statistical sensitivity for the four parts of the experimental data measured and the total weighted average of the result.

CHAPTER5

SYSTEMATIC UNCERTAINTIES

The contribution of the systematic uncertainty in measuring the expectation value of the discrete symmetry odd-operator is determined from all the steps of the selection criteria applied to the analysis. To begin with, the conditions applied on the examined data and control samples during the event selection stage may introduce bias into the final event samples, impacting the results. The impact of the applied selection criteria is investigated independently at each analysis stage by modifying the limit value of a single criterion while keeping the rest of the event selection in the same form as when the result was determined. Each of the cut values was modified based on the resolution (σ) of a variable in order to search for significant dependence of the result from a particular cut. Systematic uncertainty introduced by a given selection requirement was estimated as an average shift of the result observed as a consequence of cut variation by $\pm\sigma$. The systematic effects from each step of the data selection criteria is described in the Table 5.1. For example the standard analysis gives a result,

$$a_1 \pm \sigma_1, \tag{5.1}$$

where, a_1 denotes the result and σ_1 it's corresponding error, called Nominal Value in Table 5.1. And after making a single cut variation based on the estimated resolution of that quantity, the analysis gives a result,

$$a_2 \pm \sigma_2, \tag{5.2}$$

as described in the third column of Table 5.1. The resolution of each quantity is calculated from the reconstructed Monte Carlo signal events as described in the following section. The systematic shift from this change in the analysis is considered as the difference,

$$\Delta = a_1 - a_2. \tag{5.3}$$

For the analysis of systematic uncertainty the method described in references [93, 94] is used. As a first step the error of the observed value Δ, is estimated as,

$$\sigma_\Delta = \sqrt{(\sigma_2)^2 - (\sigma_1)^2}, \tag{5.4}$$

showing that the error is found by subtraction in quadrature of the two separate errors as described in the fourth column of Table 5.1.

Thereafter, the significance of the contribution is evaluated as,

$$Significance = \frac{\Delta}{\sigma_{\Delta}}. \tag{5.5}$$

If the significance is found to be greater than 1, the systematic shift is averaged for the positive and negative shift with the resolution and the total statistically significant systematic uncertainty contribution is estimated as the quadrature of them both [93–95].

- **Distance of the Annihilation Plane:**
  As described in Section 4.1.1, the Equation 4.7 describes the selection criteria for the distance of the annihilation plane from the annihilation position. The resolution of the quantity is derived from the Gaussian fit

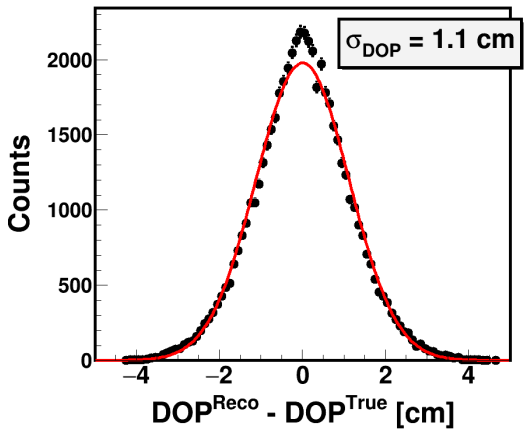

Figure 5.1: The distribution shows the difference between the reconstructed and true distance of the annihilation plane (DOP). The superimposed red curve indicates the result of the Gaussian function fit.

  to the distribution shown in Figure 5.1. Where the resolution is calculated as a standard deviation (σ_{DOP}) of

$$DOP^{Reco} - DOP^{True}$$

  distribution ie., the difference between the reconstructed and true Monte Carlo signal quantity. While performing the analysis selection criteria as described in Section 4.1.1, the DOP is calculated as

$$DOP(Analysis) = \frac{|Ax_a + By_a + Cz_a + D|}{\sqrt{A^2 + B^2 + C^2}}$$

  where the equation of the annihilation plane is given as

$$Ax + By + Cz + D = 0$$

Nominal Value: **0.0005**$\pm$0.0007		**Shifted Value**	**Aij** $\pm Sij$	**Significance**
DOP [cm] (σ_{DOP} = 1.1 cm)	1 σ	0.0007 $\pm$0.0009	0.0002 $\pm$0.0006	0.4
	-1 σ	0.0008 $\pm$0.0007	0.0003 $\pm$0.0007	0.4
Z_{Hit} [cm] (σ_{ZHit} = 2.4 cm)	1 σ	0.0003 $\pm$0.0007	0.0002 $\pm$0.0003	0.7
	-1 σ	0.0009 $\pm$0.0009	0.0004 $\pm$0.0006	0.7
θ_{i+j} [deg] ($\sigma_{\theta_{i+j}}$ = 1.5 deg)	1 σ	0.0008 $\pm$0.0009	0.0003 $\pm$0.0007	0.4
	-1 σ	0.0006 $\pm$0.0009	0.0001 $\pm$0.0006	0.1
t_{ETS} [ns] (σ_{ETS} = 0.5 ns)	1 σ	0.0001 $\pm$0.0009	0.0004 $\pm$0.0005	0.7
	-1 σ	0.0009 $\pm$0.0007	0.0003 $\pm$0.0004	0.7
TOT [ns] (σ_{TOT} = 1.2 ns)	1 σ	0.0008 $\pm$0.0007	0.0003 $\pm$0.0003	0.9
	-1 σ	0.0007 $\pm$0.0007	0.0002 $\pm$0.0004	0.5
X(Y) [cm]	1 σ	0.0009 $\pm$0.0009	0.0003 $\pm$0.0007	0.5
	-1 σ	0.0008 $\pm$0.0009	0.0003 $\pm$0.0007	0.5
Z [cm]	1 σ	0.0008 $\pm$0.0010	0.0003 $\pm$0.0007	0.4
	-1 σ	0.0009 $\pm$0.0009	0.0003 $\pm$0.0006	0.5
Edep [keV] (σ_{Edep} = 14.22 keV)	1 σ	0.0006 $\pm$0.0009	0.0001 $\pm$0.0007	0.1
	-1 σ	Insignificant down to 26 keV		
Binning —	12	0.0008 $\pm$0.0009	0.0002 $\pm$0.0006	0.4
	48	0.0007 $\pm$0.0010	0.0002 $\pm$0.0007	0.3
Cosmics —	Add	0.0008 $\pm$0.0008	0.0003 $\pm$0.0008	0.4
	Sub	0.0008 $\pm$0.0007	0.0002 $\pm$0.0008	0.3

Table 5.1: Summary of contributions to the systematic uncertainty of the measured expectation value of the discrete symmetry odd-operator at each data selection criteria. The systematic contribution from each selection criteria is explained in detail in the text.

and the annihilation point is $P(x_a, y_a, z_a)$. In order to have a symmetric distribution around zero for the accurate estimation of the resolution of DOP, the calculation was tweaked to be,

$$DOP(Resolution) = \frac{Ax_a + By_a + Cz_a + D}{\sqrt{A^2 + B^2 + C^2}}.$$

Therefore, the Figure 5.1 shows both positive and negative values of the quantity DOP.

- **Z - Interaction Hit Position:**
  As described in Section 4.1, the Equation 4.1 describes the selection criteria of the Z-interaction (hit) position for each hit along the length of the scintillator. The resolution of the quantity is derived from the double

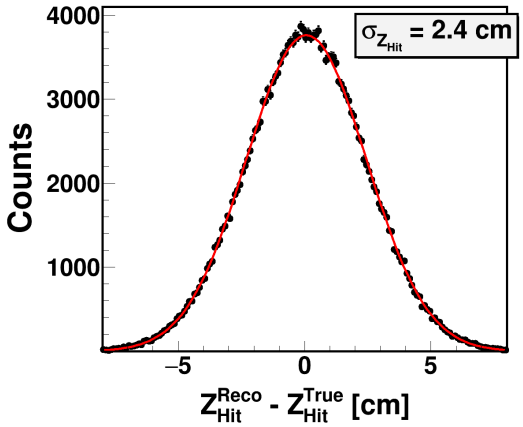

Figure 5.2: The distribution shows difference between the reconstructed and true Z-Interaction Position (Z_{Hit}). The superimposed red curve indicates the result of a double Gaussian fit.

Gaussian fit on the distribution shown in Figure 5.2. Where the resolution is calculated as a standard deviation ($\sigma_{Z_{Hit}}$) of

$$Z_{Hit}^{Reco} - Z_{Hit}^{True}$$

distribution ie., the difference between the reconstructed and true Monte Carlo signal quantity.

- **3D Angle Sum:**
  As described in Section 4.1.1, the Equation 4.8 describes the selection criteria for the sum of the two smallest 3-Dimensional azimuthal angle for an o-Ps decay.

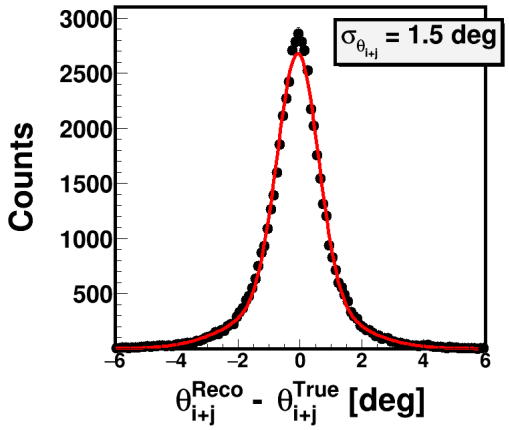

Figure 5.3: The distribution shows difference between the reconstructed and true 3-dimensional azimuthal angle sum (3D Angle Sum). The superimposed red curve indicates the result of a double Gaussian fit with corresponding standard deviations σ_1 = 0.64 and σ_2 = 1.70 and amplitudes A_1 = 10480 and A_2 = 2109, respectively.

The resolution of the quantity is derived from the double Gaussian fit on the distribution shown in Figure 5.3. Where the resolution is calculated as a standard deviation ($\sigma_{\theta_{i+j}}$) of

$$\theta^{Reco}_{i+j} - \theta^{True}_{i+j}$$

distribution ie., the difference between the reconstructed and true Monte Carlo signal quantity. Where,

$$\sigma_{\theta_{i+j}} = \frac{(w_1 \cdot \sigma_1) + (w_2 \cdot \sigma_2)}{w_1 + w_2}$$

and

$$w_1 = \frac{(\frac{1}{A_1})}{(\frac{1}{A_1} + \frac{1}{A_2})}; \qquad w_2 = \frac{(\frac{1}{A_2})}{(\frac{1}{A_1} + \frac{1}{A_2})};$$

where the derived values of A_1, A_2, σ_1 and σ_2 from the two Gaussian fits is presented in the caption of Figure 5.3.

- **Emission Time Spread:**
  As described in Section 4.1.1, the Equation 4.6 describes the selection criteria for the annihilation Emission Time Spread (ETS) for primary annihilation photons from the decay of o-Ps.

  The resolution of the quantity is derived from the Gaussian fit on the distribution shown in Figure 5.4. Where the resolution is calculated as a

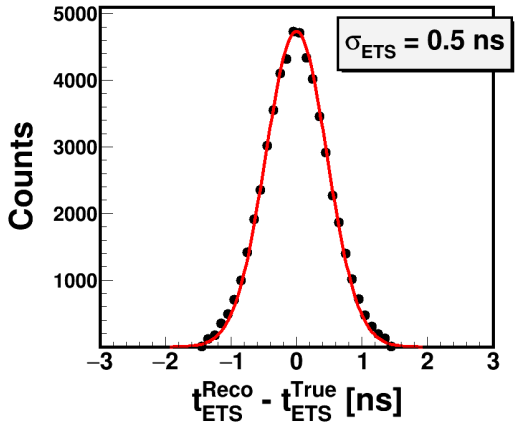

Figure 5.4: The distribution difference between the reconstructed and true emission time spread (ETS). The superimposed red curve indicates the result of a Gaussian fit.

standard deviation (σ_{ETS}) of,

$$t_{ETS}^{Reco} - t_{ETS}^{True}$$

distribution ie., the difference between the reconstructed and true Monte Carlo signal quantity.

- **Time Over Threshold:** As described in Section 4.1, the Equation 4.2 describes the selection criteria for the Time Over Threshold (TOT) for primary and secondary scattered annihilation photons from the decay of o-Ps. The left panel of Figure 5.5 shows the energy deposition of the photons in signal events (green histogram). The spectra on the right panel of Figure 5.5 shows the relationship of the energy deposition to the time over threshold for photon interaction incorporated from the article [82].

  From the Monte Carlo, the described energy deposition of the photons, where the resolution is calculated as a standard deviation (σ_{Edep}) of,

$$Edep_{Hit}^{Reco} - Edep_{Hit}^{True}$$

  distribution ie., the difference between the reconstructed and true Monte Carlo signal quantity.

  The energy deposition resolution is then translated to the TOT resolution as described in the equations below:

$$A = TOT(208keV + 14.22keV) - TOT(208keV) = 1.2\ ns$$

$$B = TOT(208keV) - TOT(208keV - 14.22keV) = 1.2\ ns$$

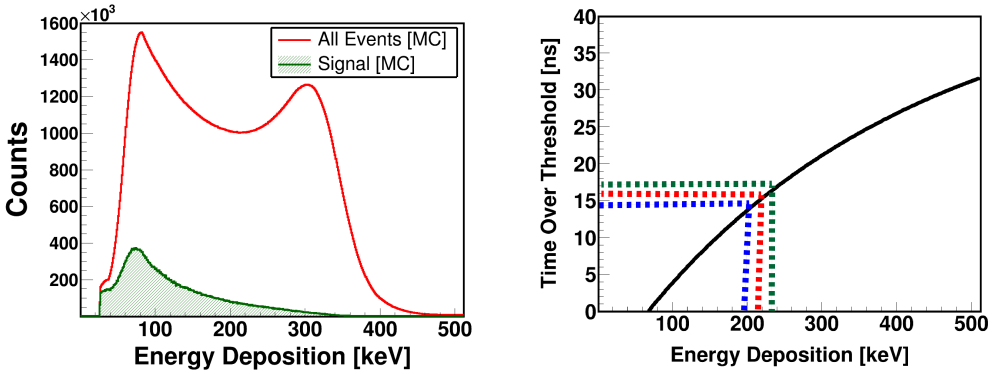

Figure 5.5: Left: Energy deposition distribution of the Monte Carlo signal events (green) and all events (red). Right: Black curve correspond to the experimental data relationship of time over threshold vs energy deposition for photon interaction [82]. The red dashed line indicates the relationship of the average energy deposition (208 keV) of the signal events to TOT. The blue and green dashed line corresponds to (208-14.22) keV and (208+14.22) keV, respectively.

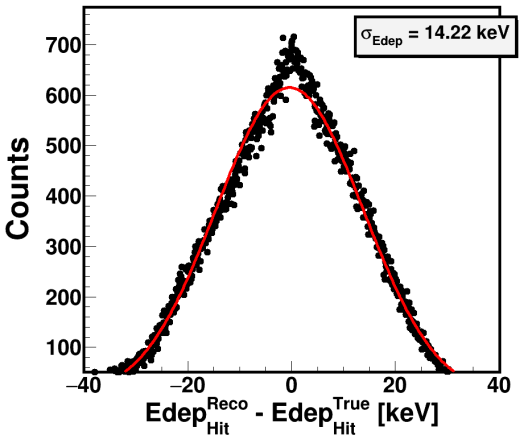

Figure 5.6: The distribution shows difference between the reconstructed and true energy deposition of the signal photons. The superimposed red curve indicates the result of a Gaussian fit.

$$\sigma_{TOT} = \frac{(A+B)}{2} = 1.2\ ns$$

Where, the energy deposition of photons is 208 keV at the TOT analysis cut value of 17 ns. The positive and negative shift of 14.22 keV as the energy resolution obtained from the fit shown in Figure 5.6 is indicated as solid

blue and green lines in the right panel of Figure 5.5.

Equations above translates the energy deposition of photons to a corresponding TOT value using the function described in the right panel of Figure 5.5.

- **Position of the Source (X, Y and Z):** The point-like source was placed in the center of the J-PET detector geometry as explained in the experiment setup description of Section 3.3. The alignment of the source plays a vital role in studying symmetries, therefore, the position of the source was reconstructed using the Line-of-Response (LOR) reconstruction method from the decay of 2-photons, from the para-Positronium events for every 25 seconds of the measurement. The experimental data and correspondingly the reconstructed Monte Carlo is corrected for the placement of the source to the exact center. Thereafter, the systematic shift in the reconstruction method in X(Y)-axis (J-PET detector is symmetric along X and Y-axes) and Z-axis is applied to both the experimental data and Monte Carlo reconstruction. The source position shifted in X(Y)-axes by $\sigma_{X(Y)}$ and the source position is shifted in the Z-axis by σ_Z.

- **Lower Energy Threshold:** As described in Table 4.1, the lower energy threshold in the Monte Carlo reconstruction is set at 31.25 keV, the resolution of the energy deposition at the lowest applied threshold is 7.7 keV which is determined from the relationship incorporated from the article [91]

$$\frac{\sigma(E)}{E} = \frac{0.044}{\sqrt{E[MeV]}}.$$

Therefore, the corresponding energy is then translated to the TOT using the function relation as shown in the right panel of Figure 5.5. The TOT resolution is then translated as described in the equations below

$$a = TOT(55keV + 7.7keV) - TOT(55keV) = 1.0\ ns$$

$$b = TOT(55keV) - TOT(55keV - 7.7keV) = 1.0\ ns$$

$$\sigma_{E_{th}} = \frac{(a+b)}{2} = 1.0\ ns$$

Where, the average lower energy deposition of annihilation photons is 55 keV. The analysis selection criteria is shifted for $\pm\sigma_{Eth}$ = 1.005 ns.

- **Binning of the Histogram:** The expectation value distribution as described in Section 4.2.2 consists of 24-bins in the range -1 to -1. The bin-width was determined based on the resolution of measuring the expectation value

from the Monte Carlo. The systematic contribution from the binning of the distribution for doubled and half of the bin size is shown in Table 5.1.

- **Cosmic Radiation Contribution:** As discussed in Section 4.1, the cosmic radiation is an inevitable background. Therefore, the cosmic radiation was scaled to the experimental measurement time to observe the influence on the final result of this study. The systematic contribution from cosmic radiation was estimated by subtracting the events of the cosmic run (normalized to the time of measurement) from o-Ps measurement. For conservative check, the effect of double the cosmic radiation events (adding events instead of subtracting) is presented in Table 5.1.

Since, none of the above investigated systematic shifts shows statistical significance [93], this experiment concludes that systematic contribution to the final expectation value measurement of the discrete-symmetry odd-operator can be neglected with respect to the achieved statistical sensitivity.

CHAPTER6

SUMMARY AND DISCUSSIONS

The aim of this thesis was to test discrete symmetries using an unique method based on the measurement of the expectation value of a discrete-symmetry odd-operator as mentioned in the first row of Table 6.1. This experiment was realised using the J-PET detector [2–6] with the operator constructed from the momentum ($\vec{k}_j$) and polarization ($\vec{\varepsilon}_i$) directions of the annihilation photons from the decay of ortho-Positronium [1]. The previous experiment testing the CP-symmetry in the charged leptonic sector was conducted in the University of Tokyo and reports the present best upper limit on the CP violation in the decays of ortho-Positronium atoms, so far [28]. The discrete symmetry odd-operator used by this research group is sensitive to the same symmetries ie., P, T and CP but the operator is constructed with the spin ($\vec{S}$) of the positronium and the momentum direction ($\vec{k}_1$ and $\vec{k}_2$) of the two most energetic annihilation photons as described in the second row of Table 6.1. Their experiment collected a total of 7.3×10^6 signal event candidates in a continuous 26-day measurement observing the expectation value to be

$$< O >_{T.\ Yamazaki\ et\ al.,} \ = \ 0.0013 \ \pm \ 0.0021_{stat} \ \pm \ 0.0006_{syst}.$$

Table 6.1: First Row: Discrete symmetry odd-operator sensitive to P, T, and CP symmetry used with the J-PET detector and reported in this thesis. Second Row: Discrete symmetry odd-operator reported experimental result from the University of Tokyo by T. Yamazaki et al., [28]

Experiment	**Operator**	**C**	**P**	**T**	**CP**	**CPT**
J-PET	$\vec{\varepsilon}_i \cdot \vec{k}_j$	+	−	−	−	+
T. Yamazaki et al.,	$(\vec{S}\cdot\vec{k}_1)\cdot(\vec{S}\cdot(\vec{k}_1\times\vec{k}_2))$	+	−	−	−	+

This thesis reports experimental measurement for 122 days in 2017-2019. The collected data is equivalent to 24×10^6 events of o-Ps$\rightarrow 3\gamma+\gamma'$ and the expectation value of the symmetry odd-operator is

$$< O >_{J-PET} \ = \ 0.0005 \ \pm \ 0.0007_{stat},$$

with no significant contribution from the systematical uncertainty and the obtained result is in agreement with the CP invariance within the achieved precision. The

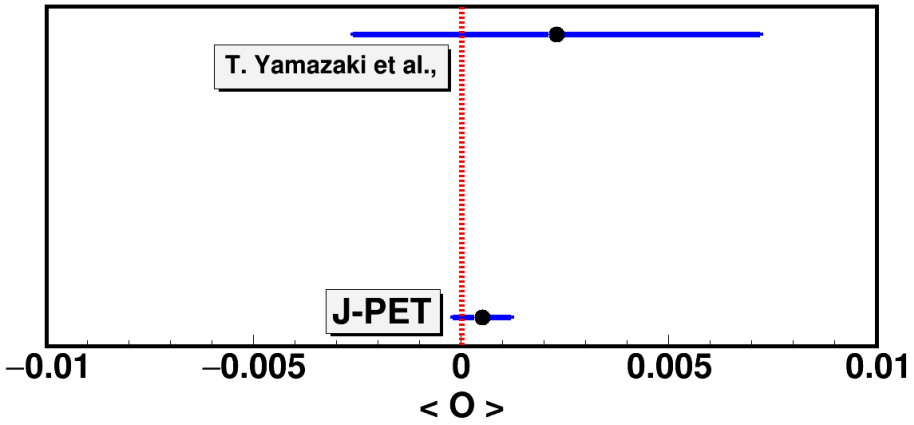

Figure 6.1: Comparison of the achieved expectation value symmetry tests with the J-PET detector with the previously published result. The red dashed line indicates no P, T and CP violation.

expectation value determined with the analysis described in this dissertation thesis is three times more precise than the best classified measurement for CP violation in the charged leptonic sector until now [28] as shown in the Figure 6.1.

As a future prospect, the J-PET collaboration has developed a modular version of the J-PET detector to improve the detection efficiency of this measurement and provide larger statistics in a shorter duration of measurement time to improve the precision significantly. The expected CP violation effects in the charged leptonic sector are highly model dependent and no single theory predicting them is known. Therefore, searches for CP violations have to be conducted through a broad range of particle systems. In this thesis more precise limitations were given for the ortho-Positronium system. Further results in this field are anticipated, among others, in neutrino oscillations [96] and atomic physics experiments [13, 51].

Bibliography

[1] P. Moskal, D. Alfs, T. Bednarski, P. Białas, et al. Potential of the J-PET Detector for Studies of Discrete Symmetries in Decays of Positronium Atom - A Purely Leptonic System. *Acta Physica Polonica B*, 47(2):509, 2016.

[2] P. Moskal, P. Salabura, J. Smyrski M. Silarski, et al. Novel detector systems for the positron emission tomography. *Bio-Algorithms and med-systems*, 7:73–78, 2011.

[3] P. Moskal, N. Zoń, T. Bednarski, P. Białas, et al. A novel method for the line-of-response and time-of-flight reconstruction in TOF-PET detectors based on a library of synchronized model signals. *Nuclear Instruments and Methods in Physics Research Section A: Accelerators, Spectrometers, Detectors and Associated Equipment*, 775:54–62, 2015.

[4] P. Moskal, S. Niedźwiecki, T. Bednarski, E. Czerwiński, et al. Test of a single module of the J-PET scanner based on plastic scintillators. *Nuclear Instruments and Methods in Physics Research Section A: Accelerators, Spectrometers, Detectors and Associated Equipment*, 764:317–321, 2014.

[5] S. Niedźwiecki, P. Białas, C. Curceanu, E. Czerwiński, et al. J-PET: A new technology for the whole-body PET imaging. *Acta Physica Polonica B*, 48(10):1567, 2017.

[6] P. Moskal .... **J. Raj** et al. Feasibility studies of the polarization of photons beyond the optical wavelength regime with the J-PET detector. *The European Physical Journal C*, 78(11), 2018.

[7] P. Moskal .... **J. Raj** et al. Testing CPT symmetry in ortho-Positronium decays with Positronium annihilation Tomography. *Nature Communications*, 12(1), 2021.

[8] P. Moskal .... **J. Raj** et al. Positronium imaging with the novel multiphoton PET scanner. *Science Advances*, 7(42), October 2021.

[9] M. Sozzi. *Discrete Symmetries and CP Violation*. Oxford University Press, 2007.

[10] E. Noether. Invariante variationsprobleme. *Nachrichten von der Gesellschaft der Wissenschaften zu Göttingen, Mathematisch-Physikalische Klasse*, 1918:235–257, 1918.

[11] P. C. Macq, K. M. Crowe, and R. P. Haddock. Helicity of the Electron and Positron in Muon Decay. *Physical Review*, 112:2061–2071, 1958.

[12] J. P. Lees, V. Poireau, V. Tisserand, J. Garra Tico, et al. Observation of Time-Reversal Violation in the B0 Meson System. *Physical Review Letters*, 109(21), 2012.

[13] K.A. Olive. Review of particle physics. *Chinese Physics C*, 40(10):100001, 2016.

[14] E. P. Wigner, Group Theory and its Application to the Quantum Mechanics of Atomic Spectra , J. J. Griffin, ix + 372 pp.,80s. *Academic Press Inc., New York*.

[15] J. H. Christenson, J. W. Cronin, V. L. Fitch, and R. Turlay. Evidence for the 2π Decay of the K_2^0 Meson. *Physical Review Letters*, 13:138–140, 1964.

[16] A. J. Buras and R. Fleischer. CP violation and rare decays after the top quark discovery. *Advanced Series on Directions in High Energy Physics*, page 65–238, 1998.

[17] M. Kobayashi and T. Maskawa. CP-Violation in the Renormalizable Theory of Weak Interaction. *Progress of Theoretical Physics*, 49(2):652–657, 1973.

[18] O. W. Greenberg. Why is CPT Fundamental? *Foundations of Physics*, 36(10):1535–1553, 2006.

[19] N. E. Mavromatos. CPT violation: Theory and phenomenology. *2nd International Conference on Exotic Atoms and Related Topics*, pages 361–372, 2005.

[20] G. Lüders. Proof of the TCP theorem. *Annals of Physics*, 2(1):1–15, 1957.

[21] H. Greaves and T. Thomas. On the CPT theorem. *Studies in History and Philosophy of Science Part B: Studies in History and Philosophy of Modern Physics*, 45:46–65, 2014.

[22] R. G. Sachs. The Physics of Time Reversal. *University of Chicago Press*, 1987.

[23] J. Bernabeu, A. Di Domenico, and P. Villanueva-Perez. Direct test of time reversal symmetry in the entangled neutral kaon system at a Φ-factory. *Nuclear Physics B*, 868(1):102–119, 2013.

[24] J. Bernabéu and F. Martínez-Vidal. Colloquium: Time-reversal violation with quantum-entangled B mesons. *Reviews of Modern Physics*, 87:165–182, 2015.

[25] W. Bernreuther, U. Löw, J. P. Ma, and O. Nachtmann. CP violation and Z boson decays. *Zeitschrift für Physik C Particles and Fields*, 43:1431–5858, 1989.

[26] B. K. Arbic, S. Hatamian, M. Skalsey, J. Van House, and W. Zheng. Angular-correlation test of CPT in polarized Positronium. *Physical Review A*, 37:3189–3194, 1988.

[27] P. A. Vetter and S. J. Freedman. Search for CPT-Odd Decays of Positronium. *Physical Review Letters*, 91:263401, 2003.

[28] T. Yamazaki, T. Namba, S. Asai, and T. Kobayashi. Search for CP Violation in Positronium Decay. *Physical Review Letters*, 104:083401, 2010.

[29] **J. Raj**, A. Gajos, C. Curceanu, E. Czerwiński, et al. A feasibility study of the time reversal violation test based on polarization of annihilation photons from the decay of ortho-Positronium with the J-PET detector. *Hyperfine Interact.*, 239(1):56, 2018.

[30] **J. Raj** and E. Czerwiński. Influence of Cosmic Radiation while Testing the Time Reversal Symmetry in the Decay of Ortho-Positronium Atoms using the J-PET detector. *Journal of Physics: Conference Series*, 1586:012010, 2020.

[31] **J. Raj** and M. Silarski. Study of the time reversal symmetry in the decay of ortho-Positronium atoms using the J-PET detector. *European Physical Journal Web of Conferences*, 199:05015, 2019.

[32] **J. Raj**, K. Dulski, and E. Czerwiński. Towards Time Reversal Symmetry Test with o-Ps Decays Using the J-PET Detector. *Acta Physica Polonica B*, 51(1):149, 2020.

[33] **J. Raj**, D. Kisielewska, and E. Czerwiński. J-PET Monte Carlo Simulations for Time-Reversal Symmetry Test in Ortho-Positronium Decay. *Acta Physica Polonica A*, 137(2):137–139, 2020.

[34] W. Barker and R. Howe. Continuous Symmetry: From Euclid to Klein. *American Mathematical Society*, 2007.

[35] E. Mottola. Symmetry and the Beautiful Universe Symmetry and the Beautiful Universe. *Physics Today*, 58(11):53–54, 2005.

[36] H. Weyl. *Symmetry*. Princeton University Press, 2015.

[37] D. Griffiths. *Introduction to Elementary Particle Physics*. John Wiley Sons, 1987.

[38] C. S. Wu, E. Ambler, R. W. Hayward, D. D. Hoppes, et al. Experimental Test of Parity Conservation in Beta Decay. *Physical Review*, 105:1413–1415, 1957.

[39] G. Q. Zhang, Z. Chen, W. Xiong, C. Lam, et al. Parity-symmetry-breaking quantum phase transition via parametric drive in a cavity Magnonic system. *Physical Review B*, 104(6), 2021.

[40] P. R. Bunker. *Fundamentals of Molecular Symmetry*. Chemical Rubber Company Press, 2004.

[41] Z. Bian, L. Xiao, K. Wang, X. Zhan, et al. Conserved quantities in parity-time symmetric systems. *Physical Review Research*, 2(2), 2020.

[42] M. Fukugita and T. Yanagida. Barygenesis without grand unification. *Physics Letters B*, 174(1):45–47, 1986.

[43] A. D. Sakharov. Violation of CP Invariance, C asymmetry, and baryon asymmetry of the universe. *Pisma Zh. Eksp. Teor. Fiz.*, 5:32–35, 1967.

[44] S. Berko, K. F. Canter, and A. P. Mills. Positronium Experiments. *Progress in Atomic Spectroscopy*, pages 1427–1452, 1979.

[45] D. C. Liu and W. K. Roberts. Experimental Search for Charge Conjugation Nonconservation in $^1S_0$ State Positronium Decay. *Physical Review Letters*, 16:67–69, 1966.

[46] J. S. Bell. Time reversal in field theory. *Proceedings of the Royal Society of London. Series A. Mathematical and Physical Sciences*, 231(1187):479–495, 1955.

[47] J. H. Christenson, J. W. Cronin, V. L. Fitch, and R. Turlay. Evidence for the 2π decay of the k_2^0 meson. *Physical Review Letters*, 13:138–140, 1964.

[48] T. D. Lee. CP Non-conservation and Spontaneous Symmetry Breaking. *Physics Reports*, 9:143–177, 1974.

[49] L. D. Landau. On the conservation laws for weak interactions. *Nuclear Physics*, 3:127–131, 1957.

[50] H. Abele, T. Jenke, E. Jericha, G. Konrad, et al. High Precision Experiments with Cold and Ultra-Cold Neutrons. *Journal of the Physical Society of Japan*, September 2015.

[51] P. G. Harris, C. A. Baker, K. Green, P. Iaydjiev, et al. New Experimental Limit on the Electric Dipole Moment of the Neutron. *Physical Review Letters*, 82:904–907, 1999.

[52] M. D. Harpen. Positronium: Review of symmetry, conserved quantities and decay for the radiological physicist. *Medical Physics*, 31(1):57–61, 2003.

[53] J. A. Wheeler. Polyelectrons. *Annals of the New York Academy of Sciences*, 48(3):219–238, 1946.

[54] A. Ore and J. L. Powell. Three-Photon Annihilation of an Electron-Positron Pair. *Physical Review*, 75(11):1696–1699, 1949.

[55] S. D. Bass. QED and Fundamental Symmetries in Positronium Decays. *Acta Physica Polonica B*, 50(7):1319, 2019.

[56] Nicola Cabibbo. Unitary symmetry and leptonic decays. *Physical Review Letters*, 10:531–533, 1963.

[57] D. N. Spergel, L. Verde, H. V. Peiris, E. Komatsu, et al. First-Year Wilkinson Microwave Anisotropy Probe (WMAP) Observations: Determination of Cosmological Parameters. *The Astrophysical Journal Supplement Series*, 148(1):175–194, 2003.

[58] R. Aaij et al. Implications of LHCb measurements and future prospects. *The European Physical Journal C*, 73(4), 2013.

[59] I. Adachi et al. Status of Belle II and Super KEKB. *Journal of Instrumentation*, 9:C07017, 2014.

[60] D. S. Ayres et al. NOvA: Proposal to Build a 30 Kiloton Off-Axis Detector to Study $\nu_\mu \to \nu_e$ Oscillations in the NuMI Beamline, 2004.

[61] K. Abe et al. Observation of electron neutrino appearance in a muon neutrino beam. *Physical Review Letters*, 112:061802, 2014.

[62] W. Bernreuther, U. Lw, J. P. Ma, and O. Nachtmann. How to test CP, T, and CPT invariance in the three photon decay of polarized $^3S_1$ positronium. *Zeitschrift for Physik C Particles and Fields*, 41(1):143–158, 1988.

[63] A. M. Baxter, T. L. Khoo, M. E. Bleich, M. P. Carpenter, et al. Compton-suppression tests on Ge and BGO prototype detectors for GAMMASPHERE. *Nuclear Instruments and Methods in Physics Research Section A: Accelerators, Spectrometers, Detectors and Associated Equipment*, 317(1-2):101–110, 1992.

[64] P. Moskal, O. Rundel, D. Alfs, T. Bednarski, et al. Time resolution of the plastic scintillator strips with matrix photomultiplier readout for J-PET tomograph. 61(5):2025–2047, 2016.

[65] A. Gajos, D. Kamińska, E. Czerwiński, D. Alfs, et al. Trilateration-based reconstruction of ortho -positronium decays into three photons with the J-PET detector. *Nuclear Instruments and Methods in Physics Research Section A: Accelerators, Spectrometers, Detectors and Associated Equipment*, 819:54–59, 2016.

[66] M. Skalsey and J. V. House. First test of CP invariance in the decay of positronium. *Physical Review Letters*, 67(15):1993–1996, 1991.

[67] P. Moskal, S. Niedźwiecki, T. Bednarski, E. Czerwiński, et al. Test of a single module of the J-PET scanner based on plastic scintillators. *Nuclear Instruments and Methods in Physics Research A*, 764:317–321, 2014.

[68] P. Kowalski, P. Moskal, W. Wiślicki, L. Raczyński, et al. Multiple Scattering and Accidental Coincidences in the J-PET Detector Simulated Using GATE Package. *Acta Physica Polonica A*, 127(5):1505–1512, 2015.

[69] O. Klein and Y. Nishina. Über die Streuung von Strahlung durch freie Elektronen nach der neuen relativistischen Quantendynamik von Dirac. *Zeitschrift für Physik*, 52(11-12):853–868, 1929.

[70] S. Flügge and L. Marton. Corpuscles and Radiation in Matter II: Vol. 34 of Handbuch der Physik. *Physics Today*, 11(11):38–40, 1958.

[71] T. Jones and D. Townsend. History and future technical innovation in positron emission tomography. *Journal of Medical Imaging*, 4(1):011013, 2017.

[72] S. Vandenberghe, E. Mikhaylova, E. D'Hoe, P. Mollet, and J. S. Karp. Recent developments in time-of-flight PET. *European Journal of Nuclear Medicine and Molecular Imaging Physics*, 3(1):3, 2016.

[73] J. S. Piotr, P. Tinsu, and G. Guido. Recent Advances and Future Progress in PET Instrumentation. 46(1):5–19, 2016.

[74] S. Surti, A. R. Pantel, and J. S. Karp. Total Body PET: Why, How, What for? *IEEE Transactions on Radiation and Plasma Medical Sciences*, 4(3):283–292, 2020.

[75] Paweł Moskal and Ewa Ł. Stępień. Prospects and clinical perspectives of total-body PET imaging using plastic scintillators. *PET Clinics*, 15(4):439–452, October 2020.

[76] P. Moskal .... **J. Raj** et al. Synchronization and Calibration of the 24-Modules J-PET Prototype With 300-mm Axial Field of View. *IEEE Transactions on Instrumentation and Measurement*, 70:1–10, 2021.

[77] W. Krzemien, A. Gajos, K. Kacprzak, K. Rakoczy, et al. J-PET Framework: Software platform for PET tomography data reconstruction and analysis. *SoftwareX*, 11:100487, 2020.

[78] R. Brun and F. Rademakers. ROOT: An object oriented data analysis framework. *Nuclear Instruments and Methods in Physics Research Section A: Accelerators, Spectrometers, Detectors and Associated Equipment*, 389(1-2):81–86, 1997.

[79] G. Korcyl, P. Białas, C. Curceanu, E. Czerwiński, et al. Evaluation of Single-Chip, Real-Time Tomographic Data Processing on FPGA SoC Devices. *IEEE Transactions on Medical Imaging*, 37(11):2526–2535, 2018.

[80] M. Pałka, P. Strzempek, G. Korcyl, T. Bednarski, et al. Multichannel FPGA based MVT system for high precision time (20 ps RMS) and charge measurement. *Journal of Instrumentation*, 12(08):P08001–P08001, 2017.

[81] L Raczyński, W Wiślicki, W Krzemień, P Kowalski, et al. Calculation of the time resolution of the J-PET tomograph using kernel density estimation. *Physics in Medicine and Biology*, 62(12):5076–5097, 2017.

[82] S. Sharma .... **J. Raj** et al. Estimating relationship between the time over threshold and energy loss by photons in plastic scintillators used in the J-PET scanner. *European Journal of Nuclear Medicine and Molecular Imaging Physics*, 7(1), 2020.

[83] M. Pawlik-Niedźwiecka .... **J. Raj** et al. Preliminary Studies of J-PET Detector Spatial Resolution. *Acta Physica Polonica A*, 132(5):1645–1649, 2017.

[84] M. Gorgol, B. Jasińska, M. Kosior, E. Stępień, and P. Moskal. Construction of the Vacuum Chambers for J-PET Experiments with Positron Annihilation. *Acta Physica Polonica B*, 51(1):293, 2020.

[85] B. Jasińska, M. Gorgol, M. Wiertel, R. Zaleski, et al. Determination of the 3γ Fraction from Positron Annihilation in Mesoporous Materials for Symmetry Violation Experiment with J-PET Scanner. *Acta Physica Polonica B*, 47(2):453, 2016.

[86] A. Pokraka and A. Czarnecki. Parapositronium can decay into three photons. *Physical Review D*, 96(9), 2017.

[87] J-PET Analysis Framework. `github.com/JPETTomography/j-pet-framework.git`. Accessed: 2022-02-01.

[88] W. Krzemień, A. Gajos, A. Gruntowski, K. Stola, et al. Analysis Framework for the J-PET Scanner. *Acta Physica Polonica A*, 127(5):1491–1494, 2015.

[89] MC simulations for J-PET using the Geant4 package. `https://github.com/JPETTomography/J-PET-geant4`. Accessed: 2022-02-01.

[90] S. Agostinelli et al. GEANT4–a simulation toolkit. *Nuclear Instruments and Methods in Physics Research Section A*, 506:250–303, 2003.

[91] D. Kamińska, A. Gajos, E. Czerwiński, D. Alfs, et al. A feasibility study of ortho-Positronium decays measurement with the J-PET scanner based on plastic scintillators. *The European Physical Journal C*, 76(8), 2016.

[92] Fred James and Matthias Winkler. MINUIT User's Guide. 2004.

[93] R. Barlow. Systematic errors: Facts and fictions. In *Conference on Advanced Statistical Techniques in Particle Physics*, pages 134–144, 7 2002.

[94] Roger Barlow. A calculator for confidence intervals. *Computer Physics Communications*, 149(2):97–102, 2002.

[95] Lloyd S. Nelson. A dictionary of statistical terms, 5th ed. *Journal of Quality Technology*, 23(2):167–168, 1991.

[96] J. Bernabeu and M. C. Banuls. CP and T violation in neutrino oscillations. *Nuclear Physics B Proceedings Supplement*, 87:315–317, 2000.

ACKNOWLEDGMENTS

First and foremost, I would like to express my gratitude to Dr. Eryk Czerwiński and Prof. Paweł Moskal, without whom this thesis would not exist. I am greatly indebted to Prof. Moskal for giving me a platform to work in his research group and constantly enhancing my career with opportunities. I am enormously grateful to Eryk, who has been my supervisor for the past years and has been unwavering in his encouragement and critical criticism.

I would also like to thank my all colleagues from the J-PET collaboration: Dr. Krzemień, Dr. Silarski, Dr. Niedzwiecki, Dr. Kamińska, Dr. Gajos, Dr. Kubicz, Dr. Skurzok, M. Pawlik-Niedźwiecka, K. Dulski, N. Chug, M. Dadgar, N. Krawczyk, F. Tayefi, Dr. Korcyl, Dr. Elena Perez del Rio and Dr. Sharma. I thank them for their companionship and providing a friendly work atmosphere.

Most importantly, I dedicate this work to my mother, Mrs. Irene Raj, for constantly believing in me and supporting me through her prayers and video calls. I thank my sister, Jyothsna Raj, and my brother-in-law S. K. Nair, who made sure I was at my most comfort being away from home and was always just a call away. To my niece, Risha Nair, for her patience and companionship through late nights of me working as she sculpted play-dough. To my grandmother, Regena Morris, for making all of this even possible through her constant support.

I am very grateful to the Świerk Computing Center in Warsaw, for providing computation resources to process and analysis experimental data and simulations for the work presented in this thesis.

This work was supported by the Polish National Science Centre through the OPUS grant Nos. 2016/21/B/ST2/01222, 2017/25/N/NZ1/00861, and 2019/35/B/ST2/03562 and the Jagiellonian University DSC grant No. 2019-N17/MNS/000036